GROWTH DYNAMICS OF ORGANIC THIN FILMS

A Thesis

Presented to the Faculty of the Graduate School

of Cornell University

in Partial Fulfillment of the Requirements for the Degree of

Master of Science

by

Sugandha Bhargava

May 2008

ABSTRACT

Organic semiconductors, in particular organic thin film transistors (OTFTs), have garnered extensive recognition and interest for several years. Their incorporation in electronic circuits has increased exponentially with major potential applications in light emitting displays and printable electronic circuits.

Thermal deposition techniques have been widely used to grow organic molecules. However supersonic molecular beam deposition has emerged as a powerful tool to study gas-surface interactions and to tune growth parameters to grow highly ordered films. With the elimination of gas phase interactions, supersonic deposition methods allows full control of the flux and the kinetic energy of the beam.

Supersonic molecular beam deposition was employed to study the effect of growth parameters on the dynamics of organic thin films. The films were grown on silicon dioxide at different growth rates ranging from 0.008 to 2 ML.s^{-1}, different substrate temperature from -66 to 60°C and at different kinetic energies from 2.7 to 6.7 eV. The films were analyzed in-situ using x-ray diffraction at Cornell High Energy Synchrotron Source (CHESS) and ex-situ using grazing incidence wide angle x-ray diffraction (GIWAXS) and atomic force microscopy (AFM). The intensity oscillations obtained as a function of time were fitted to Cohen model to obtain a set of growth parameters to understand the growth dynamics and evolution of the films.

BIOGRAPHICAL SKETCH

Sugandha Bhargava was born on 14th February 1983 in Roorkee, Uttaranchal, India. She completed her schooling at St. Ann's Senior Secondary School, Roorkee in 2000. After finishing schooling she chose to pursue Chemical Engineering at Birla Institute of Technology and Science, Pilani, Rajasthan, India in 2000. She received her Bachelor of Engineering degree in Chemical Engineering in June' 2004. In August' 2005, the author was admitted to the graduate school in the School of Chemical and Bio-molecular Engineering, Cornell University. Her focus was on understanding thin film growth with an emphasis on using x-ray diffraction as a tool to analyze the film growth. In February' 2008 she was awarded the Master's of Science degree in Chemical Engineering.

To my parents, sister and my husband

ACKNOWLEDGEMENTS

I was greatly helped by many people in the completion of this thesis and the research associated with my work. First of all I would like to thank my advisor, Professor James R. Engstrom, for introducing me to this project. His constant encouragement and guidance helped me understand and strengthen the concepts of vacuum and surface science.

I am grateful to my committee member, Prof. Joel Brock for his fruitful discussions and guidance concerning X-ray diffraction at Cornell High Energy Synchrotron Source (CHESS). His guidance during the beam time at CHESS was really fruitful. I would also like to express my gratitude to Dr. Arthur Woll for his constant time and energy during the various stages of this project. His prompt help, x-ray expertise and support with the efforts during the beam time and off-beamtime is really commendable.

I am also grateful to Dr. Detlef Smilgies for developing an understanding about GIWAXS (grazing incidence wide angle x-ray diffraction) and to use it as an analysis tool for the various film grown. I would also like to thank Dr. Aram Amassian, post doc in Malliaras group and Dr. Sukwon Hong, post doc in Engstrom group, at Cornell University, for their scientific discussions, comradeship and in helping me develop a better understanding of surface science. I am grateful to Dr. Abhishek Dube for sharing his knowledge about supersonic molecular beam deposition chamber during my early days in the research group. I would also like to thank John Ferguson who helped me in developing an understanding of x-ray diffraction and reinstalling the vacuum chamber at G-line.

Last but not the least; I am highly grateful to my parents for inculcating in me the importance of science and for always being with me through thick and thin right from elementary school all the way to graduate school. I would also like to express my gratitude towards my husband, Dr. Peeyush Bhargava, who has always been a source of support and encouragement especially during the last year of my Master's. I am short

of words to express my gratitude towards him.

This work was supported by Cornell Center for Materials Research (CCMR), a Materials Research Science and Engineering Center of the National Science Foundation. Additional support was also provided by the Nanoscale Interdisciplinary Group on Inorganic-Organic Interfaces.

TABLE OF CONTENTS

LIST OF FIGURES

LIST OF TABLES

Chapter 1
Introduction

1.1 Introduction

In 1947, John Bardeen, William Shockley and Walter Brattain, revolutionized the world of molecular electronics by the invention of transistors and replacing the vacuum tubes used in telecommunications with germanium transistors. The development of an integrated circuit from a transistor was a quantum leap in the field of electronics as integrated circuits and it formed the very basis of microprocessors which are the key component in any computer. More recently integrated circuits are being used in most of the electronic gadgets such as computers, portable electronics such as laptops, mobile phones, audio-video players; microwave ovens, flat panel displays, low end smart cards and electronic identification tags. The devices developed from integrated circuits have also been used in health care and security systems. With such an avant-garde there is hardly any industry untouched by the influence of inventions and applications in the field of electronics.

The prediction of Gordon Moore in 1965 [12], that the number of transistors will double approximately every 2 years, revised to 18 months, also brought with itself the concept of miniaturization. The exponential increase in the number of transistors has caused a steep rise in the processing speed and memory capacity. This kind of rapid development calls for continuous improvement in processing techniques and tools to manufacture devices.

1.2 Organic Semiconductors

The study of organic semiconductors dates back to early 1900's. Since then, research on organic semiconductors has gained impetus and has proven organic thin film transistors

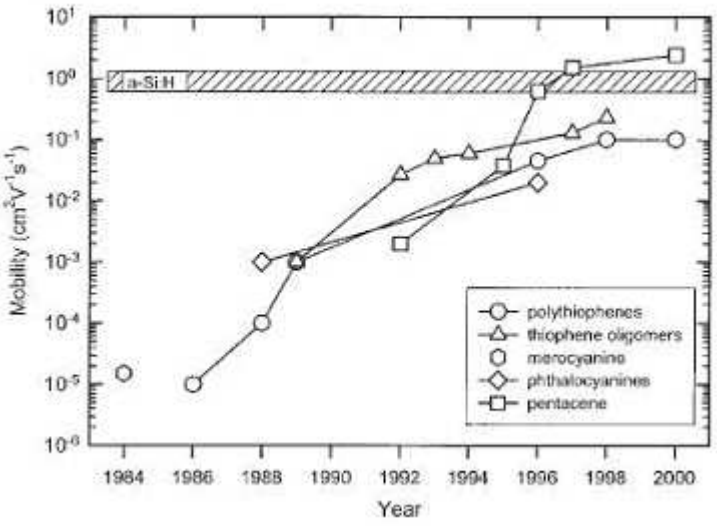

Figure 1.1: Change in the mobility of organic molecules [1].

as a viable alternative to more tradition thin film transistors based on inorganic materials such as silicon. Though the mobility of organic semiconductors can never surpass the mobility of single crystalline semiconductors such as silicon and germanium, organic semiconductors have their own advantages, which include low fabrication temperature, reduced production costs and structural flexibility. Figure 1.1 shows the increase in the field effect mobilities of the organic thin film transistors fabricated from 1986 to 2000. The electronic properties of an OTFT depend on the crystallinity of the structure. The increase in the mobility as observed in Figure 1.1 can be attributed to the new organic materials used and changes in fabrication process. Most of the organic materials crystallize at a much lower temperature, thus allowing the use of a wide variety of substrates. The above mentioned advantages of OTFTs suggest that they are a competitive tool for novel thin film application such as active matrix flat panel displays (AMFPD), active matrix liquid crystal displays (AMLCD) and active matrix light emitting diodes (AMLED) besides low end smart cards and electronic identification tags.

There have been various organic molecules, ranging from polythiophenes to poly-

acenes and fullerenes that have been used in organic thin film transistor application. Amongst them, conjugated polymers and small organic molecules are one of the most widely studies materials for organic thin film transistor applications. Small organic molecules such as pentacene have been famous because of their high mobilities amongst other organic molecules, high vapor pressure and their ability to form highly ordered thin films. The fact that the mobility of pentacene is comparable to that of amorphous silicon, along with its chemical and thermal stability and planar shape, has brought it significant attention from the world of molecular electronics. The ability of pentacene to form co-existent polymorphs (thin film phase and the bulk phase) has brought industrial attention morphology in thin film phase can be controlled by p-orbital overlap of the molecule thus governing the charge transfer and hence the mobility. Organic thin film transistor fabrication is much less complex as compared with the transistor fabrication on Si which involves high temperature and high vacuum deposition process. Low temperature deposition and use of the organic's solubility property through techniques such as spin coating and inkjet deposition have made them more popular for applications in flexible electronics.

Figure 1.2 below shows the basic schematic of a field effect transistor (FET). Most FET's are constructed from silicon wafers using single crystal semiconductor such as silicon or germanium as the active region. The gate region in a FET is the controlling region for the transfer of electrons by forming a channel between the source and the drain. One common type of FET is MOSFET (metal oxide semiconductor field effect transistor) in which the gate is metal oxide like silicon dioxide (SiO_2).

The schematic of MOSFET is shown in Figure 1.3. Pentacene has been employed as an organic semiconductor for its use in MOSFET. The performance of these electrical devices certainly depends on the deposition conditions and the interaction between the film and the substrate as they determine the crystallinity of the films which contributes

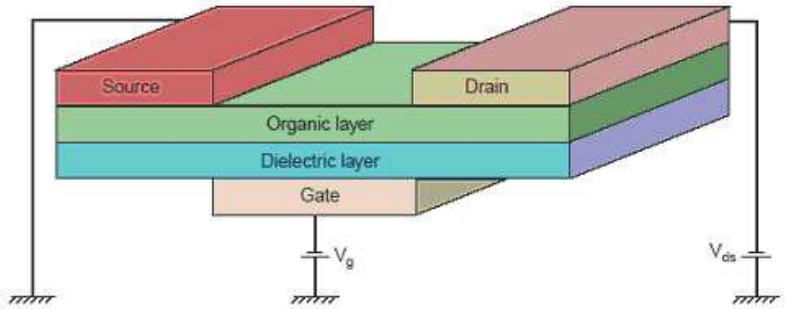

Figure 1.2: Basic schematic of a field effect transistor [2].

significantly to the charge transport. The change in the deposition conditions and/or the substrate can have a profound effect on the crystallographic structure of the film. To obtain a good charge transfer in a MOSFET, the films should have low defect and grain boundary densities and high purity. The presence of grains and grain boundaries enhance the charge trapping effect thus providing a poor charge transport lowering the mobility of the device. The semiconductor (pentacene)-dielectric (SiO_2) interface is the site of maximum charge transfer and hence it is important to understand the factors, such as surface energy, that affect the film growth process and nucleation. Devices based on small organic molecules as semiconductors are particularly interesting because the molecules are held together by weak van-der-waal forces which pose different growth dynamics as compared to covalently bonded inorganic semiconductors. For molecules such as pentacene, charge carrier properties are directly correlated with the crystalline structure, grain size, and orientation of the domains. Consequently there is a large on-going research to understand the growth dynamics of thin films of organic molecules; effect of deposition parameters to control the quality of thin films; to develop novel methods to deposit them and to make new devices on them.

The present thesis is an effort to understand the growth dynamics of organic thin films with a special attention to pentacene as the semiconductor. Effect of the deposition

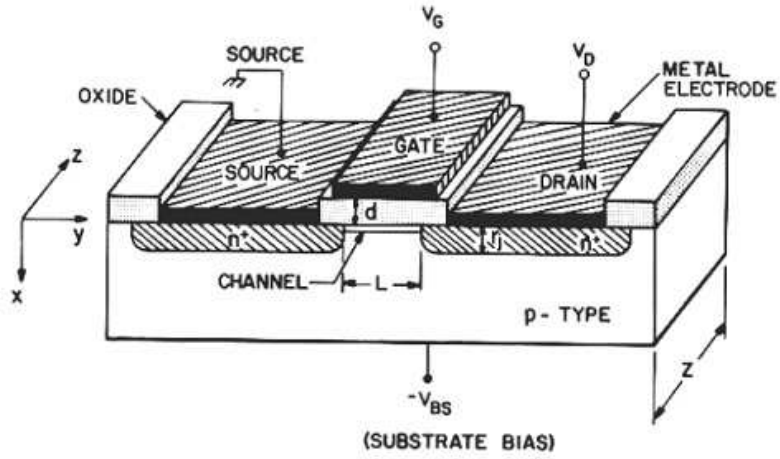

Figure 1.3: The structure of a metal oxide semiconductor field effect transistor. The substrate is usually single crystal silicon, with heavily doped source; gate oxide here is silicon dioxide [3].

parameters on the morphology of thin films have been dealt with in detail. In-situ anti-bragg scattering techniques and ex-situ atomic force microscopy (AFM) has been used to monitor early stages of pentacene thin film growth on SiO_2 and SiO_2 modified with hexamethydisilazane (HMDS). The data has been fitted to a distributed growth model to relate the experimental results with the modified version of the Cohen model.

1.3 Thin Film Deposition

The development of the semiconductor technologies depends greatly on the thin film deposition techniques. They form the very basis for developing material structures which are the foundation of semiconductor technologies such as transistors, microprocessors etc. The rapid expansion and the evolution of thin film deposition technology is attributed to the versatile applicability of the thin film devices such as organic thin film transistors, field effect transistors etc. To gain further insight into the physics and chem-

istry of growth phenomena, surface and morphology evolution, it is required to develop and improved understanding of deposition methods and the parameters that can be tuned to obtain a smooth surface.

1.3.1 Physical Deposition Techniques

As the name suggests, physical deposition methods include a physical interaction between the impinging adatom and the substrate; there is no intermediate chemical reaction involved in the process. The adatoms are either single molecules or clusters of molecules. Physical vapor deposition (PVD) techniques include molecular beam epitaxy, evaporation, pulsed laser deposition, sputtering and plasma assisted deposition. Molecular beam epitaxy takes into account the crystallographic order and the lattice matching between the film and the substrate at the interface. The molecular beam epitaxy chamber consists of Knudsen/evaporation cell in which the solid precursors are heated to a temperature at which they start evaporating to form a molecular beam. The substrate is heated to provide high mobility to the molecules for crystalline growth and also rotated to improve growth homogeneity. The use of shutter allows uniform exposure of the substrate to the precursor molecules. Molecular beam epitaxy is typically used in ultra high vacuum conditions where films with good crystal structure can be obtained at low deposition rates. Sputtering is another deposition technique where high energy particles bombard on a target material/electrode leading to the ejection of atoms which condense on the substrate as a thin film. It has been widely used to deposit metallic films on different substrates, aluminum layer for CD and DVD fabrication and anti-reflection coatings on glass. There are various types of sputter deposition such as magnetron sputtering, ion beam sputtering and reactive sputtering. Sputtering provides the ease to control the film thickness. Sputtering is advantageous over thermal evaporation due to the fact that the deposited film has the same composition as the source

material. Since sputtering provides high deposition rates, the impurity levels are much less as compared to those achieved in molecular beam epitaxy. Evaporation involves heating the source in vacuum until they evaporate, and condensing them on the substrate. Evaporation in vacuum allows source vapor to be free of any other impurities and the molecule travels in straight line, and deposits directly onto the substrate. Though evaporation has been the most classical deposition method, techniques such as sputtering and molecular beam epitaxy provide a better step coverage and hence are of more industrial significance. In pulsed laser deposition (PLD), thin film deposition happens with the ablation of material from the target in ultra high vacuum conditions by use of high energy laser beams. The high energy laser beam heats up the target material to the evaporation temperature and the ablated material moves through the plasma plume and impinges on the substrate. The energetic atoms sputter some of the atoms from the surface of the substrate, and the films start to develop after attaining a thermal equilibrium. The nucleation process, however, depends on the degree of ionization, energy of the ions among other factors. Because of its versatility, PLD has found wide applications in semiconductor industry. Electron beam deposition involves bombardment of a target anode with energetic electrons under high vacuum conditions. The energetic electron beams evaporate the material to be deposited. Electron beam deposition chambers may also be equipped with ion sources which help in etching the substrate, target sputtering and thus help in controlling the microstructure of the film. Electron beam deposition method leads to high deposition rate. Coupled with ion sources, electron beam deposition method provides high density poly-crystalline films.

In general physical vapor deposition methods provide high deposition rate, and can be used to deposit most of the inorganic materials. However there are a few disadvantages accompanied with physical deposition process, which include high capital costs, poor step coverages and difficult control of the composition of the films deposited on

the substrate.

1.3.2 Chemical Deposition Techniques

As opposed to physical deposition processes, chemical deposition process includes chemical reactions at various levels leading to the formation of the films. Different types of chemical deposition processes are electroplating, chemical vapor deposition and plasma enhanced chemical vapor deposition. Electrochemical plating techniques involve electrochemical (presence of anode which consists of the metal being plated and cathode, which acts as a source of electrons) deposition of inorganic thin films from a solution containing the metal in an ionic form. Electroless plating is used to deposit metallic films fro semiconductor applications. All the reactions occur without the use of any electrical power in the aqueous phase. Most widely used chemical deposition process in the semiconductor industry is chemical vapor deposition. It involves chemical reactions amongst the reactants in vapor phase deposition followed by the deposition of a film on the substrate. Chemical vapor deposition can be classified into various types based on operating pressure such as atmospheric pressure CVD, low pressure CVD and ultra-high vacuum CVD (UHVCVD). A modified version of CVD is plasma enhanced CVD, where chemical reactions occur after the formation of plasma by the reacting gases. Depending on whether the film is conductive or insulating, the plasma can be generated by applying either a DC voltage or a RF (AC) voltage between the two electrodes. Plasma enhanced CVD has a great advantage over thermal CVD where films have to be deposited on thermally sensitive structures. CVD has found enormous applications in integrated circuits, optoelectronic devices and dielectrics. It is advantageous where high density and high purity thin films are desired. Most of the thin films obtained by CVD are conformal. By controlling the chemistry of the reaction and deposition conditions such as substrate temperature, growth rate, flux density of the molecules, it is possible

to tune the chemical composition and the physical structure of the films. CVD processes provide uniform and high coverage of films on the substrate as reactant molecules collide multiple times before finally depositing on the substrate. Figure 1.4 pictorially represents the various steps involved in CVD process. The CVD process begins with the transport of precursors to the substrate surface. In the gas phase reactions may occur either producing reactant for film deposition or depleting the reactant intended to react on the surface. The precursor after landing on the surface decomposes or reacts to form an adatom of the growing film. The reaction by- products which are volatile in nature desorb from the surface. The adatoms may diffuse to their most probable attachment site such as a step edge. The attachement of adatoms to the step edge commences the mechanism of nucleation of new islands leading to film growth. There are many factors that control the morphology and the structure of the films formed by chemical vapor deposition processes. One of them is the operating pressure which directly affects the transport of the precursors to the surface. Since CVD involves chemical reaction, the kinetics of the reaction amongst the precursors in the gas phase and on the surface affects the process of film growth. The final morphology and the structure of the film is affected to a great extent by physical processes such as surface diffusion, nucleation of atoms on the surface, island growth, crystallization and steady state film growth. Process temperature is one of the most important determining the morphology of the films grown by CVD as it giverns the reaction rate and bulk and surface diffusion.

One of the self limiting deposition process, similar to CVD is Atomic Layer Deposition (ALD). ALD is typically used to generate conformal thin film coatings which can be used as conductors or insulators in the semiconductor industry. Usually, ALD incorporates two self limiting chemical reactions between two chemical (gas phase) precursors and a solid surface. The technique involves saturation of the substrate with one precursor, followed by the removal of the excess reactant with the help of a purge gas. The next

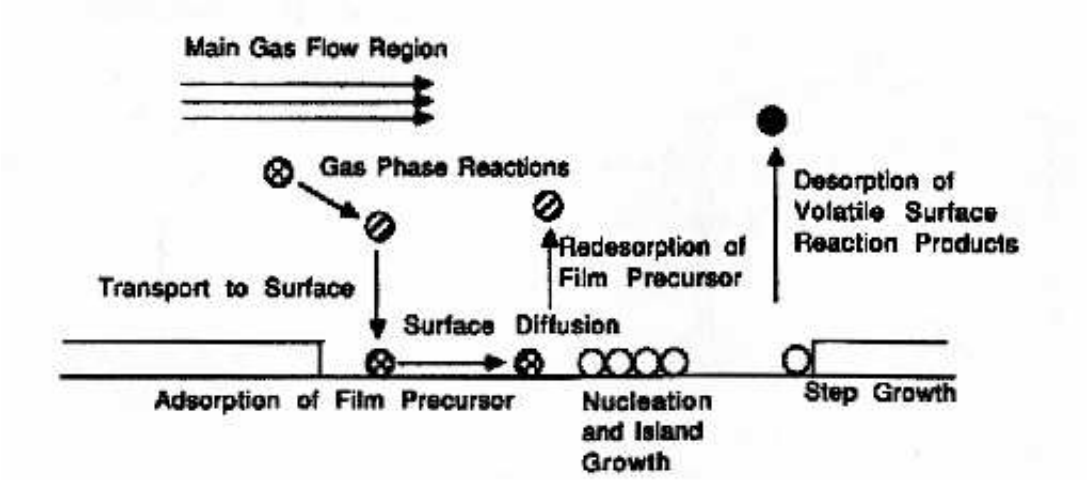

Figure 1.4: Schematics representing the mechanisms involved in chemical vapor deposition. [4].

step is to introduce the second precursor, which reacts with the first precursor to produce the desired product. The films produced by ALD are highly conformal and uniform in thickness. ALD provides an atomic scale control of the thickness of the films.The only disadvantage of ALD, as compared to CVD, is low deposition rate. Even with the low deposition rates, ALD has found tremendous applications in semiconductor industry for the formation of ultra thin films. Figure 1.5 shows a schematic representation of ALD.

1.4 Molecular Beam Techniques

The advancement in deposition techniques ranging from thermal evaporation to plasma enhanced CVD (PECVD) has fueled the aspiration to develop an understanding about the dynamics and kinetics of the interaction of molecules with different substrates. An accurate understanding of the precursor-substrate dynamics at the surface of the substrate was not apparent in most of the previously mentioned deposition techniques. In chemical deposition processes, it was difficult to co-relate the reaction kinetics with the growth of the thin films because of the gas phase reactions, multiple reactions and for-

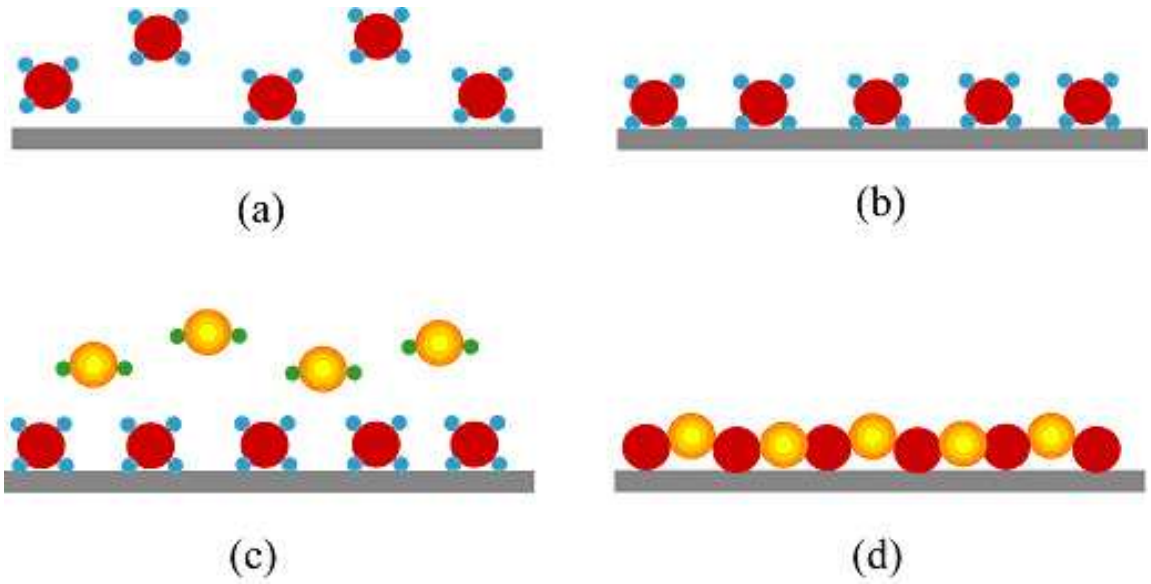

Figure 1.5: Schematic representation of the steps involved in atomics layer deposition. The first step (a) involves the precursor molecule 'A' landing on the surface of the substrate. In step (b) the precursor molecule forms a monolayer on the substrate. The second precursor molecule 'B' reacts with the precursor molecule A on the substrate to form a thin layer.

mation of intermediates. For decades, molecular beam methods coupled with surface science have been instrumental in gaining the knowledge about the gas-surface interactions and the redistribution of energy in gas-surface scattering leading to thin film growth.

A molecular beam is produced by the expansion of a gas passing through a small orifice from a region of high pressure to a region of low pressure. This produces a highly collimated beam of molecules such that the molecule-molecule and molecule-background gas interactions are negligible. Use of molecular beam methods in ultra high vacuum chambers allows precise control over various degrees of freedom such as translational, rotational, vibrational and electronic energy states besides minimizing the gas phase interactions and providing ultra-clean environments to obtain highest purity

films.

1.4.1 Characterization of molecular beams

Molecular beams are typically collimated stream of molecules, produced when a gas undergoes expansion passing through an orifice from a high pressure to a low pressure region. The molecular beams can be either classified as effusive or supersonic beams based on operating pressure and the nozzle geometries. Knudsen number (K_n) is used to characterize molecular beams and is defined as the ratio of mean free path of the molecules (λ) to the characteristic length (d). The characteristic length, d, is the diameter of the orifice for molecular beam expansion experiments.

$$K_n = \frac{\lambda}{d} \tag{1.1}$$

There are two limiting cases for Knudsen number which can be used to characterize the beams either as effusive or supersonic. For an effusive beam, $K_n \gg 1$ and the molecules tend to follow a collision free path during the expansion. The operating pressure is low enough to allow collision free transport of molecules. However molecules collide frequently with the walls of the chamber and the transport is said to be ballistic or molecular. For a supersonic beam, $K_n \ll 1$ and the mean free path of the molecules is much smaller as compared to the characteristic length. In such a case, molecules undergo various collisions and the transport is said to be continuum.

Effusive molecular beams

As discussed above, effusive molecular beams (Figure 1.6) involve collision free transport of molecules. The non-interactive transport between the molecules and the beam characteristics such as internal and translational energies are governed by kinetic theory of gases and hence are characterized by Maxwell Boltzmann distribution. The flux

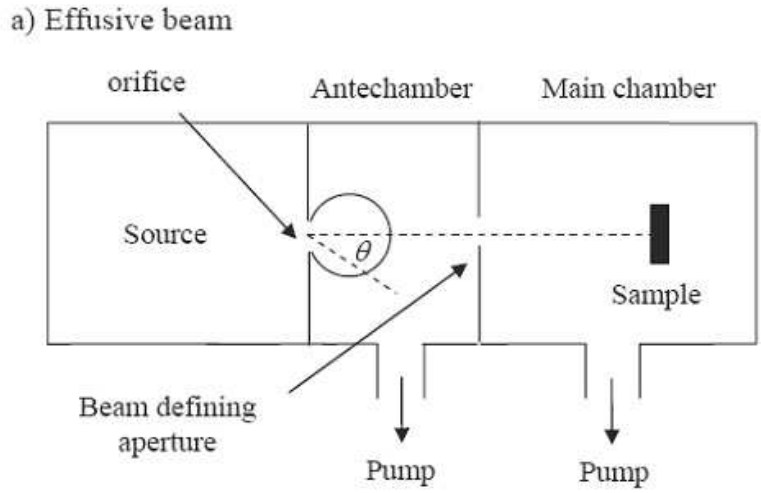

Figure 1.6: Schematics for an effusive molecular beam [5].

weighted velocity distribution for the molecules in an effusive beam along the beam axis is given by:

$$F(v) = \left(\frac{2}{(\frac{2k_BT_n}{m})^2}\right) v^3 exp\left(\frac{-v^2}{(\frac{2k_BT_n}{m})}\right) \tag{1.2}$$

Here T_n is the source temperature, k_B is the Boltzmann constant and m is the molecular weight of the molecule. The average translational energy ($< E_i >$) of an effusive beam is $2k_BT_n$ which shows that the effusive beams have low energy. The energy rises up to few hundred eV when the nozzle temperature is raised by a few hundred $^\circ C$. Owing to the low energy of the effusive beams, they affect the thin film growth. Since the effusive beams cannot be collimated, it becomes difficult to use them to study gas-surface interactions. The disadvantage of low flux and low beam to background ratio can be overcome with the help of supersonic molecular beams.

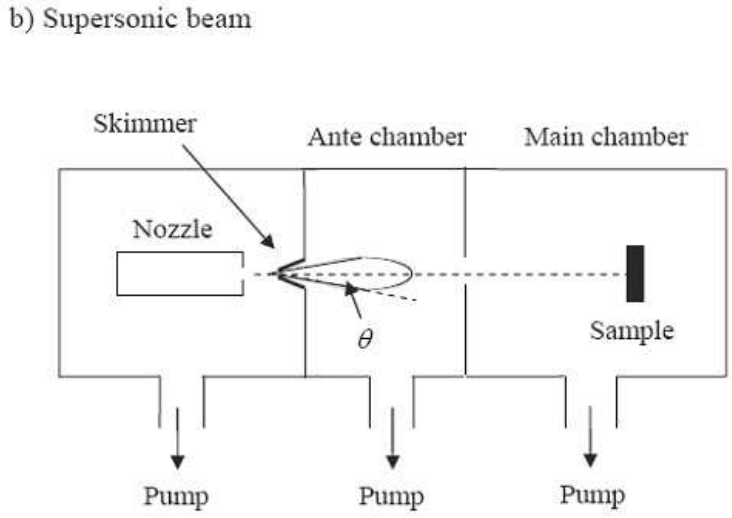

Figure 1.7: Schematics for a supersonic molecular beam [5].

Supersonic molecular beams

Supersonic molecular beams (Figure 1.7) are produced when the mean free path of the molecules is much smaller than the characteristic length ($K_n \ll 1$). The molecules undergo collisions during an isentropic expansion while exiting from a nozzle at high pressure. Due to collisions, thermal energy of the molecules is transferred as the kinetic energy of the molecules which is directed along the beam axis. Therein lays the advantage of supersonic beams as they allow wide range of translational kinetic energies with narrow distribution of velocities. Based on the fluid flow conditions, the spatial distribution of the beam shows $\cos 4\theta$ dependence, which implies a peaked distribution. The presence of a peaked distribution is significant in studying the gas surface interactions necessary to understand the thin film growth phenomena. Figure 1.8 pictorially shows the supersonic expansion. The molecules moving at a low velocity accelerate due to the pressure gradient as the nozzle area decreases.

The flux weighted velocity distribution for a supersonic beam is much narrow and is

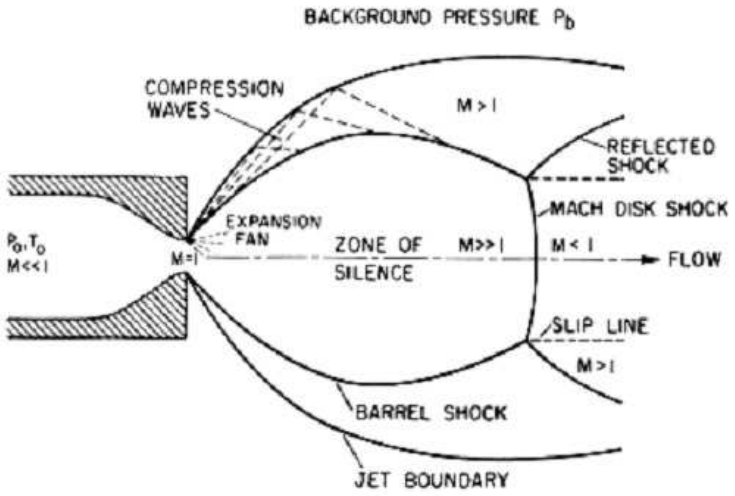

Figure 1.8: Schematics of structures formed from supersonic molecular beam expansion [6].

given by:

$$I(v) \sim v^3 exp(\frac{-m(v - v_0)^2)}{2k_B T_{jet}}) \tag{1.3}$$

Here T_{jet} is the static temperature in the beam/jet or the axial translational temperature, k_B is the Boltzmann constant, v_0 is the most probable velocity. The static temperature of the jet is a major parameter governing the velocity distribution of the supersonic beams. As compared to the equation for velocity distribution of effusive beams, T_{jet} is much lower than T_n, temperature of the source. As shown in Figure 1.8, molecules (having a thermal velocity upstream of the nozzle) in the stagnation state at a pressure P_0, are accelerated by the imposed pressure gradient (pressure downstream, P_b = vacuum of the nozzle) to sonic speeds. The molecules attain sonic speeds given by:

$$s = (\frac{\gamma k_B T_n}{m})^{0.5} \tag{1.4}$$

If the ratio of the pressure upstream of the nozzle, P_0, to the background pressure (pres-

sure downstream of the nozzle(P_b)) satisfies:

$$\frac{P_0}{P_b} > (\frac{\gamma+1}{2})^{\frac{\gamma}{\gamma-1}} \tag{1.5}$$

To obtain sonic speeds in the expansion, it is important to consider another parameter, called the Mach number (M) which is defined as ratio of the gas velocity to the speed of sound. In order to attain sonic speeds, the pressure ratio should be such that the Mach number is greater than 1. Supersonic molecular beams have an advantage to attain higher beam energies by seeding a dilute mixture of heavy molecules in a light carrier gas such as helium, hydrogen, nitrogen. In a seeded supersonic beam, all the molecules are accelerated to the same velocity. The average translational energy of the heavy molecule seeded in a light gas is given by:

$$< E_i >= \frac{m_i}{m} < C_p > T_n \tag{1.6}$$

Here m_i is the mass of dilute molecule, $< m >$ is the average molar mass of the gas mixture, T_n is the nozzle temperature and $< C_p >$ is the average molar heat capacity of the mixture. The kinetic energy of the supersonic beam can be increased by increasing the nozzle temperature as well as through the seeding techniques. However, increasing the nozzle temperature increases the translational and the vibrational energy of the molecules. Thus an appropriate combination of the two parameters (nozzle temperature and the carrier gas) can tune the internal states of the molecules to obtain uniform films.

Supersonic molecular beams allow independent control over translational, rotational, electronic and vibrational states of the molecules along with ability to deposit uniform films on small substrates. It allows better control of flux and minimizes the reactions between the molecules in gas phase. The seeding technique used in supersonic beams provides a wide range of translational energies. The advantages of supersonic beams coupled with their use in ultra high vacuum systems help in maintain ultra clean environments thus maintaining film purity levels. Supersonic molecular beams coupled

with in-situ and ex-situ analysis techniques are being employed constantly to grow device quality film and to understand the chemical and physical kinetics of the process.

1.4.2 Supersonic Molecular Beam Scattering

Supersonic molecular beams have been widely used to grow device quality films and to understand the dynamics of the film deposition process involving gas-surface interactions. During the film deposition process, the impingement of the molecule may or may not lead to chemical changes in the scattered or the absorbed species. Kinetic energy of the incident molecules, chemical nature and the reactivity of the molecules with the substrate determine if the molecule has changed chemically. Based on the above discussion, the scattering process can be classified into reactive and non-reactive scattering processes.

Non-reactive Scattering

Non-reactive scattering involves no chemical interaction between the molecules and the substrate and the incident molecules have the same composition as the incident molecules. It does not contribute to the film growth, but is important in determining the physical state of the surface and the interaction between the molecule and the surface. There are different events that a molecule can undergo when it impinges on the surface such as adsorption, desorption and scattering. Non-reactive scattering can be classified as elastic scattering, inelastic scattering, molecular trapping and desorption, and molecular chemisorption.

Elastic scattering

Elastic scattering involves conservation of the energy of the incident molecule. The molecule impinges on the surface and is scattered without any loss in translational or

vibrational energy. It allows the molecules to interact with the substrate for a very small period of time (i.e. the residence time of the molecule on the substrate is very less 10-12 sec). Though elastic scattering doesn't contribute to film growth dynamics, it provides information about the substrate topology.

Inelastic Scattering

Inelastic scattering involves transfer of energy between the impinging molecule and the substrate, i.e. the kinetic energy of the molecules is not conserved. The energy transferred from the molecule can either change increase the internal energy or can lead to the generation of phonons. The molecules can loose energy by one collision (direct inelastic scattering) or by multiple collisions (indirect collision scattering) with the substrate. Due to multiple scattering the molecules tend to have an angular distribution. As opposed to elastic scattering, the residence time of the molecules, which is determined by the number of collisions by the impinging molecules on the substrate, is larger.

Trapping (Physisorption) or desorption

Trapping or physisorption is the phenomena which involves interaction between the molecules and the substrate by long range attractive van-der-waal forces. The incident molecules adsorb (get trapped) on the substrate and equilibrate at the surface i.e. the molecules reach a thermal equilibrium before desorping. The molecule's desorption from the substrate is governed by Maxwell-Boltzmann distribution characterized by the temperature of the substrate and is not controlled by the energetics. The strength of trapping is controlled by the adsorption energies, which are a function of substrate temperature. At higher substrate temperature, molecules with lower adsorption energies undergo desorption. Since the incident molecules are trapped and undergo thermalization, the residence is higher as compared to direct scattering.

Molecular chemisorption

Molecular chemisorption involves formation of a chemical bond between the molecule (while retaining their identity) and the substrate as opposed to trapping where the incident molecules are held by weak van-der-waal forces. The adsorbed molecules are held strongly with the binding energies of the order of 1-10 eV/atom as against 50-500 meV/atom in physisorption. Since chemisorption involves the formation of a chemical bond, the potential energy well is much deeper which indicates a higher residence time of the adsorbed molecule on the substrate.

1.5 Thin film deposition using supersonic molecular beams

Supersonic molecular beams have been used significantly to understand the gas-surface interactions to fathom the dynamics of processes involved in thin film growth. They provide high intensity and directionality to the beams thus allowing the growth of uniform films at very high growth rates. Supersonic molecular beams provide an unprecedented control over structural, morphological and hence the function properties of the thin films. Incident kinetic energy, flux distributions, angle of incidence, substrate temperature are the prime parameters which can be tuned using supersonic molecular beams to obtain uniform films of high purity. In addition flux densities are much higher as compared to the vapor deposition methods. Various chemical processes such as plasma-enhanced CVD (PECVD) and self limiting processes such as atomic layer deposition can be activated at low temperatures. Owing to their unique advantages, supersonic molecular beam method employed as an independent technique or in conjugation with other techniques such PECVD, ALD, can be used to get a deeper insight into film growth processes such as nucleation and island formation. Supersonic molecular beams have been used to deposit inorganic materials such as Ge on GeAs(100) [13] for organic materials

such as pentacene, tetracene on SiO_2 [10,14] and metals such as Ag(111) [15]. More recently supersonic beams have been used for cluster deposition leading to morphological changes for developing device quality films.

1.6 Molecular beam of clusters

Clusters are formed when molecules are held together by weak van-der-waal forces. Molecular beam of clusters have been an area of intense research activity for many years. Energetic clusters have known to give rise to more uniform morphology and better quality films [16], however they prove to be vexing when it is important to study an isolated molecule [17]. Owing to the continuously changing growth parameters such as pressure and temperature in supersonic expansion, it is difficult to theoretically model cluster formation in supersonic beams because of the strong temperature dependency of the kinetic parameters. In addition the cluster density varies non-linearly with the monomer density. The nucleation and the process of island growth continuously release the heat of condensation leading to increasing temperatures and thus decreasing Mach numbers. The non-equilibrium conditions of the supersonic molecular beam expansion give rise to cluster formation. Hagena and Obert reported that the cluster formation in expanding supersonic jets depend strongly on pressure, temperature, carrier gas and the size of the nozzle. An increase in the nozzle diameter allows more collisions during the expansion and thus leading to more clustering. It was also shown that under the effect of supersonic (isentropic) expansion, the mean cluster size remained constant if the pressure and the temperature of the source are increased simultaneously [18]. The cluster nucleation strongly depends on pressure and commences when the local pressure is higher than the corresponding vapor pressure at that temperature. This condition where local pressure in the nozzle is higher than the vapor pressure at that temperature is called supersaturation. The increase in the stagnation pressure shifts the point of

supersaturation upstream of the nozzle, thus causing more collisions and hence leading to the formation of larger clusters. In seeded molecular beams, concentration of the inert species also affects monomer collisions leading to cluster formation.

The size distribution of the clusters in the molecular beam is significant because measuring size distributions help in characterizing, developing and improving control over molecular beam cluster sources and also understand the process of nucleation in supersonic expansion. More recently the observation of intensity discontinuities at different cluster sizes have been correlated with the dynamics of nucleation, stability of geometric and electronic structures and fragmentation and ionization of clusters during various size distribution measurements. Clusters have been quantified using electron impact ionization mass spectrometry. Though mass spectrometric method has yielded extensive information on cluster size distribution owing to its advantages such as high sensitivity, low background noise and compatibility with other experimental techniques. However, one major disadvantage of mass spectrometry is extensive fragmentation of clusters into smaller clusters and monomers, which can give a distorted signal and hence a distorted ion size distribution as compared to the cluster size distribution in the parent beam. This makes it difficult to relate the measured signal with the cluster size distribution [19]. One of the methods devised by Buck and Meyer determines the cluster size distribution using the kinetic constraints in elastic scattering of argon clusters by using a cross molecular beam of helium. They measured the angular and the velocity distribution of scattered clusters and related them with the original cluster mass. It was shown that fragmentation is a predominant and argon clusters fragment into monomers and dimers [19, 20].

Besides the above mentioned short-comings mass spectrometry has been used to determine cluster size distributions. The intensity of m/e=278 and m/e=556 which correspond to a pentacene monomer and dimer of a direct modulated beam, were measured

for a 150μm nozzle. The formation of clusters as observed by the intensity of m/e=556 was observed at a bubbler temperature of $280^{\circ}C$ at which the nozzle pressure was 800 torr. The nozzle pressure seemed to be much higher as compared to the pressure observed in the normal regime which is around 55 torr. This suggests that clustering may happen at high nozzle pressures. As shown in chapter 6, calculation of a dimensionless parameter, C^*, confirms the formation of clusters in molecular beam of helium seeded with pentacene. Even though the intensity of the dimers is much lower as compared to that of the monomers, it is believed that there is a little cluster formation in the pentacene beams. Additional insight whether molecular clusters are bound by van-der-waal forces or chemical interactions are currently a topic of research.

1.7 X-ray diffraction

The analysis of organic and inorganic thin films has been done by various ex-situ techniques such as atomic force microscopy, scanning electron microscope and in-situ techniques such as x-ray diffraction (XRD). Owing to the non-destructive nature of x-rays, in-situ x-ray diffraction has been widely used to analyze thin films and study interfaces and surfaces. X-ray diffraction is an essential surface characterization tool because x-rays interact weakly with matter which avoids multiple scattering from the surface and they can penetrate deep into the matter (depending on the energy) thus giving microscopic structural information. Since x-rays have wavelengths of the order of a few angstroms, comparable to interatomic distance in crystalline solids, they are used for analyzing materials which are crystalline in nature and have regular repeating structures. This gives x-ray diffraction an upper hand over other scanning techniques which are restricted to surface and interfaces and cannot give high resolution while scanning a large area simultaneously.

1.7.1 Bragg diffraction

Synchrotron based x-ray diffraction is a powerful technique to reveal information about the crystallinity of the film, crystallographic structure, average domain size and film orientation. X-rays have been used to analyze samples such as DNA, protein structure besides organic and inorganic thin films. Based on the shape of the intensity curves, one can also extract information on dislocation density and surface roughness. They can be either absorbed or scattered upon interacting with the matter. The scattering of x-rays from a crystal lattice is governed by the Bragg's law, which is defined as

$$m\lambda = 2dsin\theta \tag{1.7}$$

where m is an integer, λ is the wavelength of the x-rays, θ is the angle of incidence to the lattice plane and d is the spacing between two planes. The incoming x-rays can interfere either constructively or destructively with the lattice planes (Figure 1.9). In Bragg diffraction, scattered intensity is observed, when path length between the scattered x-rays from adjacent crystalline planes is equal to an integral number of x-ray wavelengths. In the anti-Bragg diffraction as opposed to Bragg diffraction, x-rays from the adjacent planes interferes destructively (the reflected waves from two adjacent planes are π out of phase).

Figure 1.10 represents the geometry for specular diffraction from which information about the crystalline planes parallel to the surface can be extracted. The crystal truncation rods contain a lot of information about the crystalline structure. A crystal extending infinitely throughout the space would diffract beams at sharp points in reciprocal space. However the surface of a real crystal truncates in space. The diffraction pattern and the substrate giving rise to the diffraction pattern are related by Fourier Transform. The fact that the surface of a real crystal truncates can be taken into account by multiplying a step function with the crystal lattice and hence the Fourier transform of the truncated crystal produces streaks of intensity through every reciprocal lattice point. As we have seen for

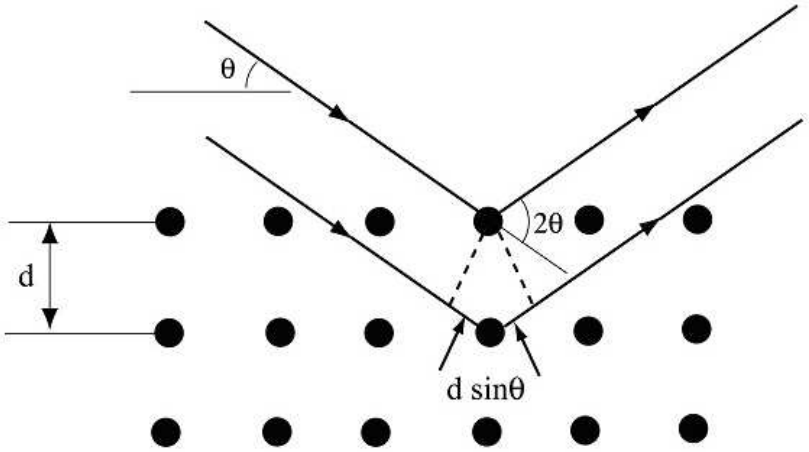

Figure 1.9: Bragg's diffraction. The two diffracted waves which are π out of phase represent anti-bragg scattering.

most of the specular reflection (reflectivity measurements), the intensity dropped precipitously until the anti-Bragg position and then rises sharply near the Bragg peak (001 peak).

Anti Bragg scattering occurs when the reflected waves interfere destructively (i.e. they are p out of phase) has been used to monitor early stages of pentacene thin film growth on SiO_2 and modified SiO_2 with HMDS. In other words, the momentum transfer or the wave vector is such that

$$q.d = \pi \tag{1.8}$$

where d is the inter-planar spacing. It is also called as 0,0,1/2 reflection since it occurs at half the angle of Bragg scattering. The scattered intensity from the n^{th} layer will cancel the intensity from the $(n-1)^{th}$ layer. The importance of anti-bragg scattering lies in the fact that destructive interference makes the surface more sensitive and hence it has been used before to monitor the growth for both organic and inorganic films [21].

Rocking curve is another scan that reveals information about in-plane geometry and

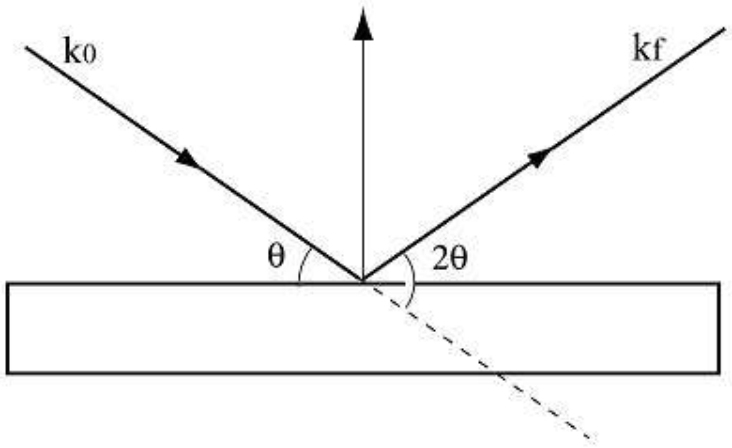

Figure 1.10: Specular diffraction revealing information about the ordering parallel to the substrate.

length scales. The angle μ(reflected angle) is rocked over a narrow angular range keeping the incident angle θ fixed. Rocking curves reveal information about the strains in the films and the width of the rocking curve gives information about the sample surface curvature.

1.7.2 X-ray reflectivity (XRR)

X-ray reflectivity (specular and diffuse scattering) is an important tool to gather information about the roughness of the surface as it is an important parameter to determine the quality of the interfaces. Since x-rays pass from air to a reflecting medium (with refractive index < 1), it is possible that the x-rays might be totally reflected if the incident angle (between the sample surface and the incident beam) is small. This is the condition of total external reflection. The smoothness of the surface determines the fraction of x-rays transmitted or reflected from the surface. For a flat surface, the reflected intensity is confined in a direction symmetric to the incident beam (which implies that the exit

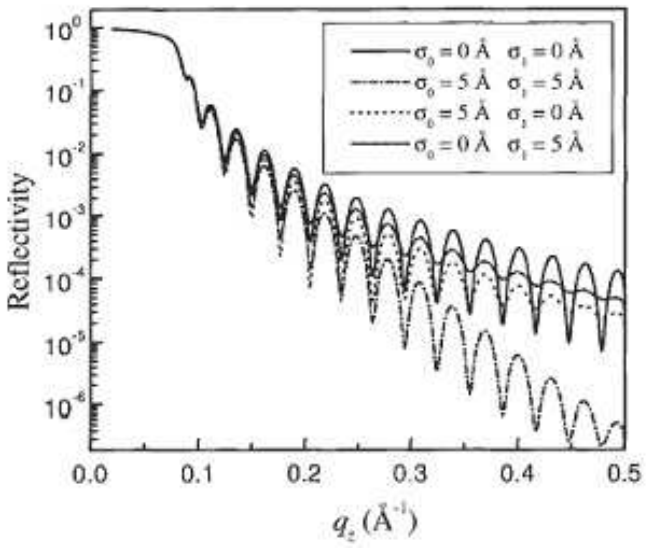

Figure 1.11: Influence of the substrate and the surface roughness on the reflectivity of thin film of gold deposited on silicon substrate [7].

angle is the same as the incident angle) and this is called as specular reflection. Conventionally, it can be defined as the ratio of the reflected intensity ($I(\theta)$) to the intensity of the incident beam (I_0).

$$R(\theta) = \frac{I(\theta)}{I_0} \tag{1.9}$$

In the conditions of specular reflectivity, wave vector 'q' has its parallel components q_x and q_y as zero while the component in the perpendicular direction , $q_z = 4\pi sin\theta/\lambda$. The technique of specular reflection plays a significant role when the surface has defects and is rough. Rough surface have a tendency to reflect less than a flat and smooth surface. Thus surface roughness, (σ), can be related to the specular intensity. The effect on the specular intensity when a surface is rough versus when it is smooth is shown below in Figure 1.11.

The fundamentals of specular intensity are useful when the surfaces are flat. For a perfect crystal, the scattered intensity would consist of discrete set of Bragg reflections. However, as mentioned above, for rough surfaces, one has to consider off-specular (dif-

fuse) scattering. Diffuse scattering gives information about the lateral correlations and about the crystal disorders as the wave vector is non-zero in the directions parallel to the surface. In order to determine diffuse scattering intensity, one has to know the form of height-height correlation function. Diffuse scattering provides information about the roughness of the interface between the film and the substrate and also between the layers of films. Thus x-ray reflectivity measurements (specular and diffuse scattering measurements) are an important tool to understand the interfaces, surface structures, determine the roughness and layer thickness and thus provide complete information about the morphology of the films and the crystallographic structure.

1.7.3 Grazing incidence X-ray diffraction (GIXD)

Grazing incidence x-ray diffraction is another diffraction technique which gives information about the in-plane structure such as the crystallographic structure, strain in the films etc. As mentioned before, x-rays can be used to study the bulk material as well as the surface. If the bulk is a single crystal, the scattering is limited to the Bragg peaks. To obtain additional information about the structures developed on the surface, one can observe the scattering between the Bragg peaks. In reciprocal space this corresponds to the scattering from surface crystal truncation rods (CTR), which has been discussed in the previous section. In order to gain significant information from the crystal truncation rod analysis, it is important that there is little scattering between Bragg peaks. In the case of thin substrates, it is difficult to analyze the films by CTR analysis as the substrate is transparent to the x-rays. Due to averaging over multiple orientations, it can result in the loss of the information about the lateral structure.The set up of grazing incidence x-ray diffraction is shown in Figure 1.12.

Grazing incidence x-ray diffraction is a surface selective technique and avoids scattering from the substrate. It combines Bragg condition with the condition of total ex-

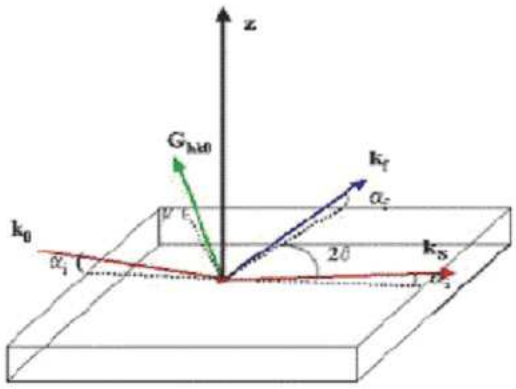

Figure 1.12: Grazing incidence x-ray diffraction revealing in-plane structure of thin films.

ternal reflection from crystal surfaces. Total external reflection is observed when the incident angle is very small and the refractive index is less than 1.0. At the condition of total external reflection, substrate is slightly visible to the x-rays and hence the penetration is much less, thus the highest intensity is observed at this condition. This prevents penetration of the x-rays into the crystal and provides lateral and in-plane information about the morphology of the films. Through grazing incidence diffraction very thin films deposited on the substrates become accessible. The limitation of using GIXD is that it mostly works well with smooth surfaces, and not all surfaces to be studied are smooth.

1.8 Cohen Model

During the growth of thin films, there are various parameters that govern the film morphology and the crystallographic structure. The complexity of the model increases as the number of parameters governing the film growth increase. Synchrotron x-ray scat-

tering provides a technique for the real time monitoring of the growth. The intensity versus time data and the reflectivity measurement reveal a lot of information about the crystallographic structure. The information obtained from these curves can be fitted using a model to obtain information about the layer coverage with time, roughness of the films, critical coverage for coalescence, island shape and the magnitude of Ehlrich-Schwoebel barrier. Based on the kinematical approximation, the X-ray intensity for specular reflection by a thin film is given by:

$$I \propto \mid r_{sub} e^{-i\phi} + r_{film} \sum_{n} \theta_n e^{-iqd_n} \mid^2 \tag{1.10}$$

Here r_{sub} is the reflection amplitude of the substrate; r_{pent} is the reflection amplitude from a layer of the film, θ_n is the coverage of the n^{th} layer of the film, θ_{total} is the total coverage, q is the momentum transfer, d is the layer spacing of the pentacene film, and ϕ is the phase difference between the waves reflected from the substrate and from the first layer of the film. For anti-bragg scattering,

$$q.d = \pi \tag{1.11}$$

and the scattered intensity is measured along (0,0,1/2) reflection. This implies destructive interference of the waves reflecting from n^{th} and the $(n-1)^{th}$ layer. At the condition of anti-bragg scattering, the surface becomes more sensitive and this is represented as intensity oscillations as the films grows and nucleates above the substrate. To model the thin film growth process for multi-layers it is important to understand the processes involved in the formation of first monolayer followed by processes involved film evolution and nucleation for the growth of multi-layers. Pentacene molecules impinging on the surface for the formation of first monolayer can undergo various processes such as adsorption (1), desorption (2), surface diffusion (3), nucleation (4), and attachment (5) to other molecules or to a step edge, as shown in the Figure 1.13. The fate of the molecule is decided once it lands on the surface. Based on what kind of interaction the molecule

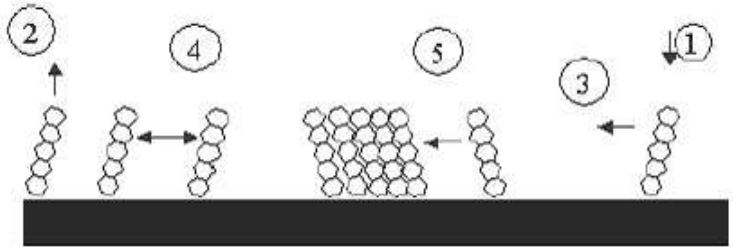

Figure 1.13: Pentacene molecules undergoing different processes after impacting the substrate [8].

undergoes, it can lead to layer by layer (2D) growth or 3D growth. Nonetheless, it also depends on the deposition parameters. From anti-bragg scattering, it is possible to monitor real time whether molecules undergo 2D or 3D growth. For a 2D growth, where the surface is smooth and less number of islands are formed, more oscillations are observed. For a 3D growth, the oscillations die out relatively quickly. For modeling the growth beyond the first monolayer, it is important to understand the mechanisms involved in the formation of upper layers. Rate equation approach becomes more complex due to the increased number of parameters involved in the film growth process. However models related to surface sensitive techniques are more useful and provide significant information about in-plane structures and inter-layer transport which play a major role in the formation of smooth films. The formation of upper layers can involve mechanisms such as an admolecule diffusing to become a part of the step edge. Such mechanisms are complex and involve a barrier called as the Ehlrich-Schwoebel (E-S) barrier which is defined as the difference between the step down barrier and the diffusion activation energy. E-S barrier control the ease of layer by layer growth.

Birth-death models, proposed by Cohen [9], have been used to model film growth beyond the first monolayer. It uses a set of non-linear differential equations and gives

surface coverages during growth which provides significant information for the formation of islands while modeling the growth of several monolayers. It keeps track of the relative coverages and interlayer transport thus providing significant information about the in-plane structure. Cohen proposed several equations to model epitaxial growths and incorporated possibilities that an adatom landing on the n^{th} layer can diffuse and thus incorporate at the step edge of the $(n+1)^{th}$ layer, or transfer down one level and join the n^{th} layer. Two mechanisms that were neglected are thermal desorption and upward funneling of the molecules from the n^{th} layer to the $(n+1)^{th}$ layer. One such model that incorporates these is the distributed model. Figure 1.14 below represents the distributed growth model. As described by Cohen the equation of the coverages for the distributed model is given by:

$$\frac{d\theta_n}{dt} = (\nu - \nu_n^{des})(\theta_{n-1} - \theta_n) - \nu\alpha_{n-1}(\theta_{n-1} - \theta_n) + \nu\alpha_n(\theta_n - \theta_{n+1}) \tag{1.12}$$

where θ_n is the coverage for the n^{th} layer, ν is the deposition rate, ν_n^{des} is the rate of desorption from the n^{th} layer, α_n measures the rate at which the molecule is being transferred from the $(n+1)^{th}$ layer to the n^{th} layer (inter-layer transport).Since desorption from the surface and from the islands (a phenomena that does not happen until the substrate temperature is $> 60\ ^\circ C$) has been neglected, ν_n^{des} is zero. The equation1.12 becomes:

$$\frac{d\theta_n}{dt} = \nu_{eff}(\theta_{n-1} - \theta_n) - \nu_{eff}\alpha_{n-1}(\theta_{n-1} - \theta_n) + \nu_{eff}\alpha_n(\theta_n - \theta_{n+1}) \tag{1.13}$$

The term $\nu_{eff}(\theta_{n-1} - \theta_n)$ represents the number of adsorbates landing on top of (n-1) layer per unit time. Since α_{n-1} is the probability at which the molecule transfers from n^{th} layer to the $(n-1)^{th}$ layer, $(1 - \alpha_{n-1})$ is the probability at which the molecules remain on top of $(n-1)^{th}$ layer. Similarly the last term in the equation, $\nu_{eff}\alpha_n(\theta_n - \theta_{n+1})$, represents the fraction (α_n) of the molecules that transfer from $(n+1)^{th}$ layer to the n^{th} layer. The inter-layer transport, α_n, can be expressed in terms of the island perimeter of the n^{th}

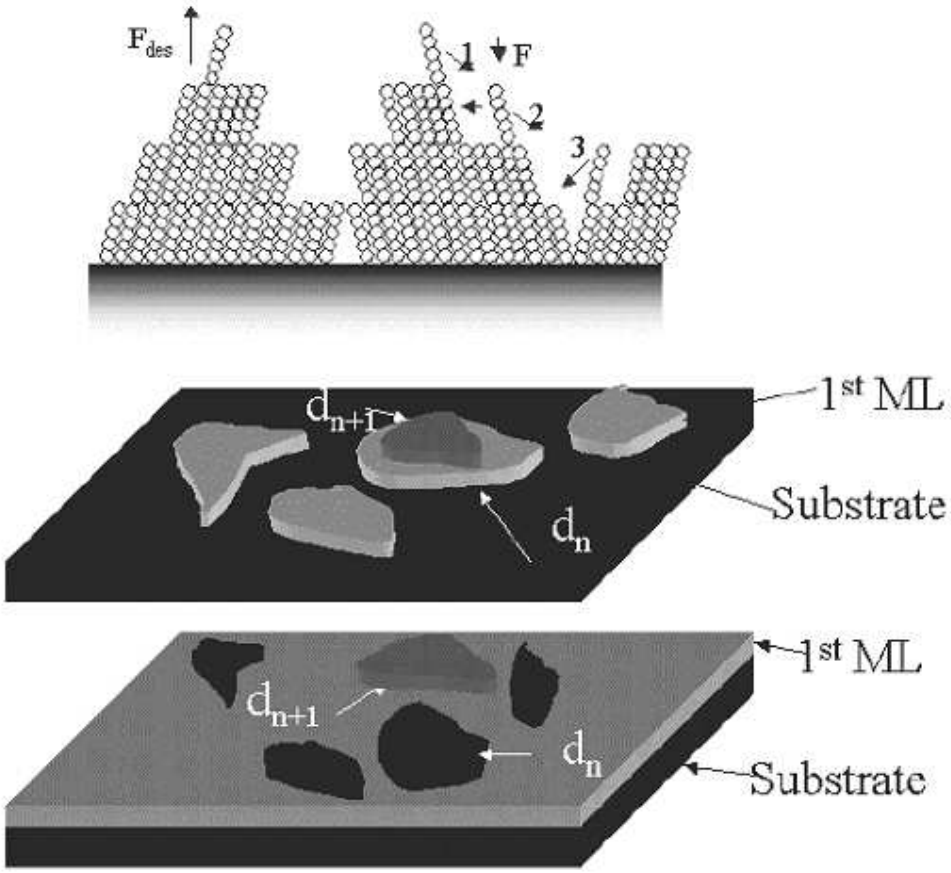

Figure 1.14: Relevant growth parameters as considered by the distributed growth model for the growth of thin film beyond the first monolayer. The first figure shows the pentacene molecules on SiO_2 substrate showing the deposition rate F, and the desorption rate F_{des} [9].

layer as:

$$\alpha_n = A\frac{d_n(\theta_n)}{d_n(\theta_n) + d_{n+1}(\theta_{n+1})} \tag{1.14}$$

where 'A' accounts for the probability of the molecule hopping down from the $(n+1)^{th}$ layer to join the n^{th} layer. Thus the factor A is a function of E-S barrier. The two limiting cases for 'A' are for a perfect layer by layer growth, when A = 1 and for a non-diffusive growth, when A = 0. For d_n or $d_{n+1} = 0$, $\alpha_n = 0$. The perimeter of an island (d_n) on the n^{th} layer is related to the layer coverage of the n^{th} layer. Assuming that there exists

same number of holes in the film with the same perimeter, when the surface is less than or more than half filled, d_n as a function of θ_n is represented by:

$$d_n(\theta_n) = \theta_n^{p1} \qquad \text{for } \theta_n < \theta_c$$

$$d_n(\theta_n) = (1 - \theta_n)^{p2} \qquad \text{for } \theta_n > \theta_c \tag{1.15}$$

θ_c is the critical coverage at which coalescence occurs. It is observed that the damping in the intensity oscillations is large when the second layer starts to form before the first layer is completed. The number of intensity oscillations is indicative of a layer by layer growth for the first few monolayers. The number of oscillations and the amplitude of the oscillations decrease quickly as the upper layers start to form before the lower layers are complete. For the deposition of pentacene on SiO_2, the peak intensities correspond to an integral number of layers, and the oscillation show a cusp like character which is indicative of high diffusion and inter-layer transport.

Chapter 2
Literature review

2.1 Pentacene as an organic molecule for thin film growth

Among the various organic molecules being studied, pentacene (Figure 2.1(a)), a planar five benzene ring molecular system [10], is a promising organic semiconductor owing to its high field effect mobility [22] and its ability to form highly ordered thin films [1] (Figure 2.1(b, c)) on variety of substrates. Pentacene is a p-type semiconductor with mobility values reported as 1 $cm^2V^{-1}s^{-1}$ making it a direct competitor of amorphous Si [1,22]. Pentacene is known to have two molecules per unit cell arranged in a herringbone configuration. It has been found that pentacene exists in thin film phase and bulk phase. The molecule has a triclinic structure in bulk phase as shown in Figure 2.1

The bulk polymorph is found to co-exist with the thin film phase in vacuum evaporated films beyond a certain thickness. The p orbital overlap in pentacene determines the charge transport properties and hence it is important to understand the molecular packing in pentacene thin films. The crystalline structure of pentacene thin films has been reported by x-ray diffraction [23]. Specular diffraction yields information about the inter layer spacing perpendicular to the substrate. Powder diffraction pattern of pentacene films reveal information about the domains/grains having their unit vectors a, b parallel to the surface but being randomly oriented with respect to each other.

Pentacene has been deposited by various deposition methods such as thermal evaporation, ion assisted deposition, pulsed laser deposition and more recently by supersonic molecular beam deposition. It is known to grow in a herringbone configuration and have two polymorphs [24]. However the formation of different polymorphs, their configuration in the film and the crystallinity of the films depends largely on the deposition parameters and the substrate condition. Pentacene has been grown on a variety of sub-

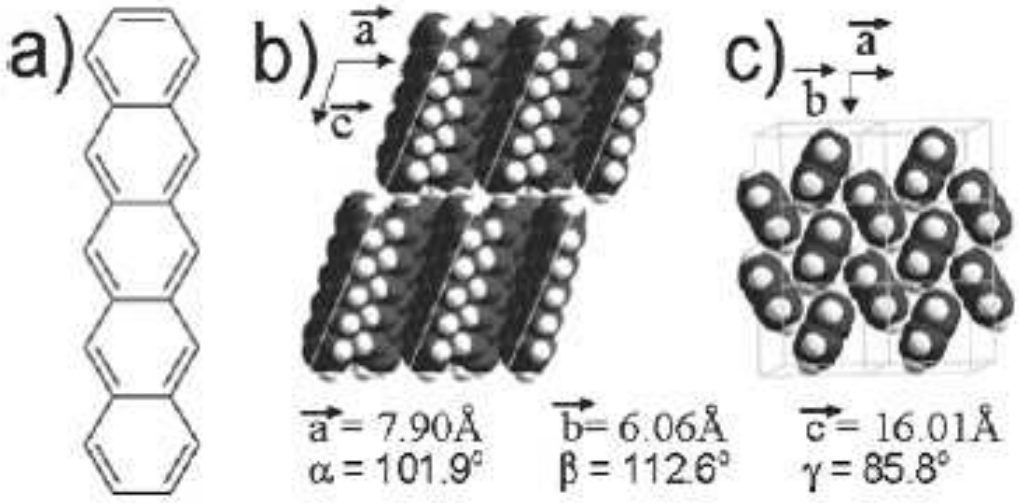

Figure 2.1: (a) Structure of pentacene (b, c) bulk crystalline structure of pentacene [10].

strates such as surface modified with hexamethyldisilazane (HMDS), copper, modified gold surfaces and more commonly thermally grown SiO_2. Kafer and co-workers studied the molecular orientation and crystallinity of pentacene films grown on Au(111), polycrystalline gold and gold substrates modified with self assembled monolayers of organothiols. The molecules tend to grow in a planar fashion constituting the wetting layer, and then continue to grow in a tilted fashion [25]. It has been reported that surface modification with HMDS significantly affect the film morphology in the sub-monolayer regime. Pentacene grown on substrates modified with hexamethyldisilazane (HMDS) have shown heterogeneous nucleation, trapping mediated growth and a higher island density than for pentacene grown on SiO_2 [26]. Ruiz and co-workers have reported the growth of pentacene on Ag (111) at 200K and proposed a diffusion mediated growth of pentacene with a critical island size of four molecules [27].

Although the interactions between the molecules and the inorganic substrate are either weak van-der-waal interactions or hydrogen bonding, the crystallographic phase,

the degree of orientation and the morphology of the resulting film depends on the substrate film interface and the kinetics of growth. It has also been shown that deposition conditions have a significant effect of the morphology of thin films. Substrate temperature, growth rate and kinetic energy of the incident beam play a major role in morphology, crystallinity and grain orientation thus affecting the field effect mobility of the thin films. Tejima and co-workers studied the effect of pentacene thin films for a temperature range (223 - 342K) and found that the pentacene growth follows a diffusion mediated growth model with a critical island size of two at low temperatures and a critical island size of three at high temperatures. The diffusion mediated model has been more commonly used for inorganic thin film growth [28]. Knipp and co-workers studied the effect of deposition rate and the substrate temperature on the transport properties of pentacene thin films. Pentacene films grew in a herringbone structure when they were deposited on a smooth silicon nitride (dielectric) surface. It was found that decreasing the deposition rate increases the crystalline bulk phase of the material [29]. It was reported that the critical grain size increases with an increase in temperature; however the diffusion rate is not affected significantly by an increase in temperature [30].

There have been few studies till date conducted on the transistors formed from energetic deposition of pentacene molecules [31]. Iannotta and co-workers [14] reported the increase in crystal size of pentacene deposited on SiO_2 from 100-200 nm to 1-2 μm with an increase in the incident kinetic energy from 0.3 eV to 5.5 eV , with the latter films yielding transistors with mobility of 0.5 $cm^2V^{-1}s^{-1}$. The nucleation of pentacene thin films on bare SiO_2 deposited at high incident kinetic energies was analyzed and the incident kinetic energy was strongly found to influence the process of adsorption thus affecting the island density [32].

2.2 Pentacene polymorphs and the phenomena of clustering

Organic thin films have been characterized by ex-situ methods such as atomic force microscopy, scanning electron microscope and in-situ methods such as x-ray diffraction. Being non-invasive and non-destructive, in-situ x-ray diffraction is widely used to characterize thin films.

Pentacene is known to have two phases, thin film and bulk phase. The thin film phase is more prominent in vacuum evaporated films [33] and the bulk polymorph is found to co-exist with the thin film phase beyond a certain thickness [34]. The p orbital overlap in pentacene governs the electronic and the transport properties of pentacene thin films and hence it is important to understand the morphology and the growth mechanism to get good field effect mobility. More recently, the use of pulsed laser deposition and supersonic molecular beam deposition has resulted in a better control of growth parameters thus affecting the morphology and structure of thin films. It has been shown that pentacene tends to form polymorphs when the growth conditions are varied and films are grown beyond a certain thickness, bulk phase coexist with the thin film phase. It was reported that pentacene tends to form two polymorphs in the bulk phase at ambient pressure. It was determined through grazing incidence x-ray diffraction of vacuum deposited ultra thin films that the polymorphism in the films depends on the film thickness and the substrate temperature [35]. The consistency of the inter-planar d_{110} spacing of the two polymorphs (in ultra thin films and 100nm thick films) confirmed that the bulk phase grows on the thin films phase. Mattheus and co-workers determined the formation of two new pentacene polymorphs other than the thin film and the bulk phase, one with a d_{001} spacing of 14.1 Å grown from vapor transport, and the second being 15.0 Å [36]. The polymorph with d-spacing of 14.1 Å is formed in single crystals of pentacene. Wu and Spence determined that the formation of different polymorphs depends largely on the crystal growth conditions. They found that the 15.1 Å polymorph exists at deposi-

tion at high growth rate at room temperature followed by annealing at 473K while the 13.9 Å polymorph was formed at a low deposition rate at 353K without annealing [37]. Chapter 6 of this thesis further describes the existence of a new polymorph which was formed at high deposition rate and high incident kinetic energies.

2.3 Formation of clusters

Recent studies, as mentioned above, show that change in the deposition parameters such as deposition rate (governed by nozzle pressure), substrate temperature, carrier gas flow rate (determining incident kinetic energy), can lead to significant changes in the film morphology. Supersonic molecular beam deposition gives freedom to tune foremen-tioned parameters to obtain films with a smooth morphology which can give high field effect mobility. Hagena and co-workers founded that the cluster sizes in the cluster beams (molecular beams which undergo expansion in vacuum and van-der-waal forces hold molecules together) are a strong function of nozzle diameter, shape, temperature and nozzle pressure. They found that the cluster size almost remained constant with increasing nozzle temperature if the nozzle pressure was simultaneously increased [18]. The deposition of pentacene cluster beams on untreated and pretreated SiO_2 surfaces with hexamethyldisilazane (HMDS) by neutral cluster beam deposition method has been studied by Abthagir and co-workers with AFM and x-ray diffraction (XRD). They found that highly smooth single crystalline films were produced and the presence of the HMDS enhances the crystallinity. Organic thin film transistors formed on clean SiO_2 and SiO_2 treated with HMDS have shown significantly improved mobilities of 0.19 and 0.31 $cm^2V^{-1}s^{-1}$ [38]. The smoothness of the cluster assembled films depend on the cluster sizes and the energy with which they impinge on the surface. It was found that small clusters align epitaxially on a smooth surface when cluster deposit at thermal energy, while large clusters tend to form grains. To achieve complete contact epitaxy

and a smooth surface, multiple cluster deposition is preferred over single cluster deposition. The substrate temperature plays a significant role in surface smoothing as cluster hillocks tend to flatten at temperatures between 300-500K [39].

Iannotta and Milani [40] found that molecules deposited by hyperthermal cluster beams from supersonic seeded sources provide the ability to tune the morphology, structure and the functional properties of thin films by controlling the energy and the momentum of the source parameters. The energy of the clusters is a function of the carrier gas and the expansion conditions. They used supersonic beams of C_{60} seeded in He, thus giving them a kinetic energy between 30-50 eV and found smaller grains with less number of defects. Park and co-workers determined that the grain size of pentacene deposited by ion-cluster beam deposition (ICB) on a polyimide surface were larger than those reported by conventional deposition methods which was the cause of increased mobility of devices made from films deposited by ion cluster beam deposition [41]. It was also found that energetic cluster beams can lead to additional changes in the chemistry of the cluster molecules and they even tend to react with the surface [42]. Hyperthermal cluster beams impact film morphology remarkably by the process surface smoothing. It has been observed that the energetic clusters impinging on the surface form craters and the ejected atoms have a significant lateral momentum [43, 44]. The high energy of the molecules lead to rapid surface diffusion and hence surface smoothing. Energetic impacts of gas cluster ions at a slope through sputtering lead to the downward motion of the ejected atoms and thus surface smoothing is enhanced [43,44].

Based on earlier findings, it is evident that the structure and the morphology (governed by grain size, density of defects) of thin films controls the transistor properties. Beam parameters such as beam energy, momentum allow an unprecedented control of the film morphology. Hyperthermal cluster deposition plays a significant role in smoothing of the surface. Supersonic molecular beam deposition method is very promising as

it allows tuning of beam parameters such as kinetic energy (by changing the carrier gas), high intensity and directionality thus allowing the deposition of epitaxial films at high growth rates. The use of supersonic deposition method favors a better control on cluster deposition producing smoother films. Chapter 6 further explains formation of clusters and new polymorphs formed during the supersonic deposition of pentacene on SiO_2.

Chapter 3
Deposition of organic thin films

Organic thin films have been deposited by thermal deposition and supersonic deposition methods. This chapter talks about the supersonic beam chamber description and its specifics.

3.1 Supersonic molecular beam chamber description

Deposition of pentacene thin films at various growth rates, substrate temperatures and helium flux (beam energy) was carried out in a custom designed ultra high vacuum chamber at Cornell High Energy Synchrotron Source (CHESS). The side view of the chamber is shown in Figure 3.1. The chamber is divided into three main sub-chambers - source, ante and main, with a separate load-lock assembly. There is a gate valve that isolates the load-lock from the main chamber and helps in loading and unloading the sample without venting the supersonic molecular beam chamber.

The source chamber has the bubbler assembly which carries the molecule to be deposited (such as pentacene). The bubbler is directly connected to gas delivery lines at one end and to a nozzle (150 μm aperture) at other end. The nozzle, bubbler and tube connecting nozzle and bubbler are heated using tungsten ribbon heaters, encased in ceramic tubing. Carrier gases such as helium or nitrogen are used to produce supersonic molecular expansions of organic molecules such as pentacene. These gases are fed to the system using MKS mass flow controllers. The vapors of organic molecules are seeded in the carrier gases, which then exit the nozzle through 1/8" heatable stainless tubing. This nozzle-bubbler assembly (Figure 3.2) is mounted on a precision x-y-z manipulator and the temperatures of the nozzle (T_n), bubbler (T_b) and 1/8" tube section (T_t) can be monitored independently using K-type thermocouples spot welded to their surfaces.

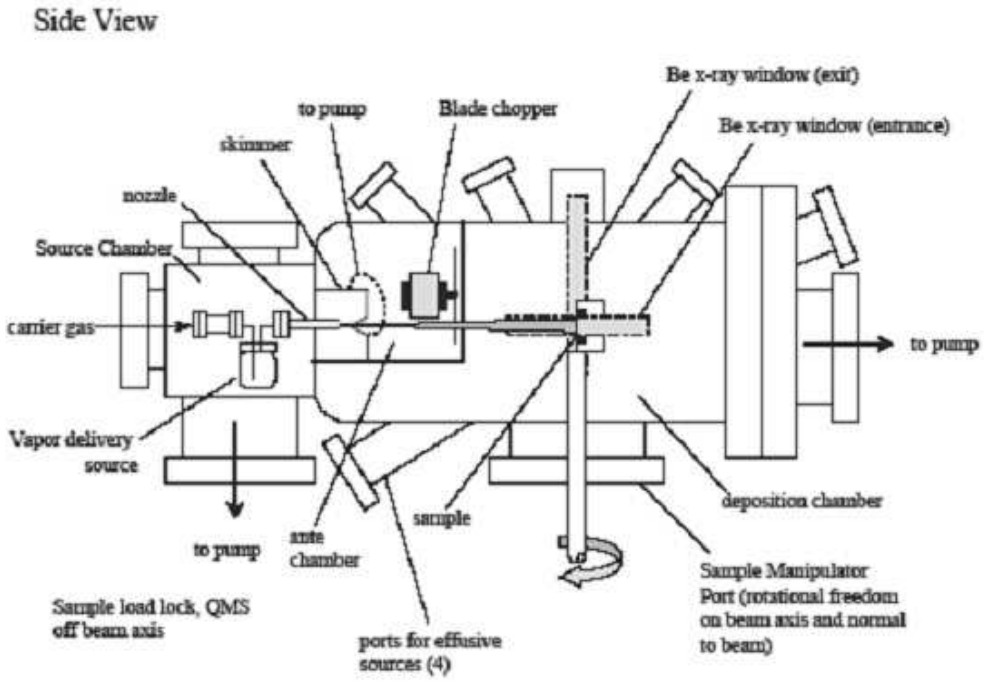

Figure 3.1: Side view of gas deposition system (G-line system) [11].

The source chamber is pumped using a 520 Ls^{-1} corrosion resistant turbomolecular pump (Pfeiffer TMU 520C). The gas mixtures (pentacene vapor and carrier gas), exiting from the nozzle expands into the source chamber. The expanded gases pass through a trumpet-shaped Ni skimmer (2.0 mm in diameter) mounted on a stainless steel plate and into the antechamber. The source and the main chamber are separated from each other by an antechamber, which allows differential pumping and further collimation of the beam before it enters the main chamber. The main purpose of the antechamber is beam modulation, which is done through an aperture plate. A reciprocating beam flag in the antechamber chops the molecular beam from the skimmer, which allows precise exposure of the sample to the beam. The beam is further collimated using the aperture plate, before entering the main chamber shown in Figure 3.3. The antechamber is pumped by a high throughput turbomolecular pump (Blazers TPU 62H). There is an

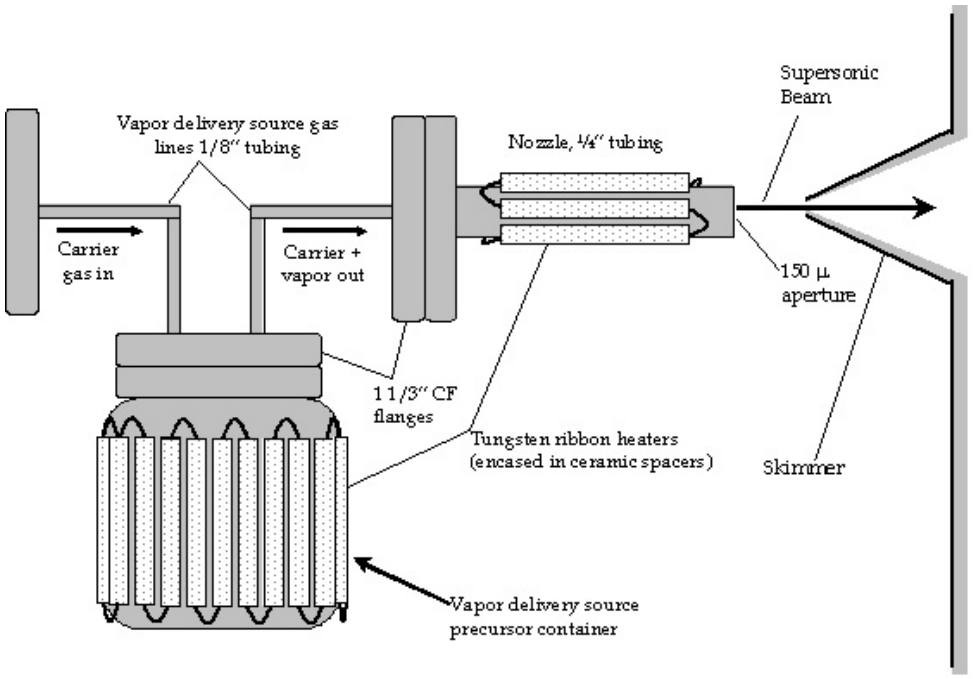

Figure 3.2: Bubbler assembly in the supersonic molecular beam chamber [11].

annulus shaped liquid nitrogen shroud connected to the antechamber which further aids in pumping down the condensable gases. However for in-situ anti-bragg measurements this shroud was taken off, and not much difference in the rocking scans was observed. Main chamber is located adjacent to the antechamber, where thin films are deposited on various substrates. The main chamber is pumped by a 400 Ls^{-1} turomolecular pump (Osaka TG 403M) and it achieves a base pressure of 5 x 10^{-10} Torr.

The substrates are mounted in platens made out of Molybednum (Mo). The sample is 2.68" away from the aperture plate. Due to small distance between the aperture plate and the sample, the gas source should come through the antechamber to avoid very low angles of incidence to the sample. The sample (Thermionics), capable of z movements as well as rotational motion in the azimuthal direction (zeta axis) and polar (normal to the beam axis - theta axis) movements holds the sample holder in place. All motions are controlled by motors. There are two rectangular Be windows, placed opposed to

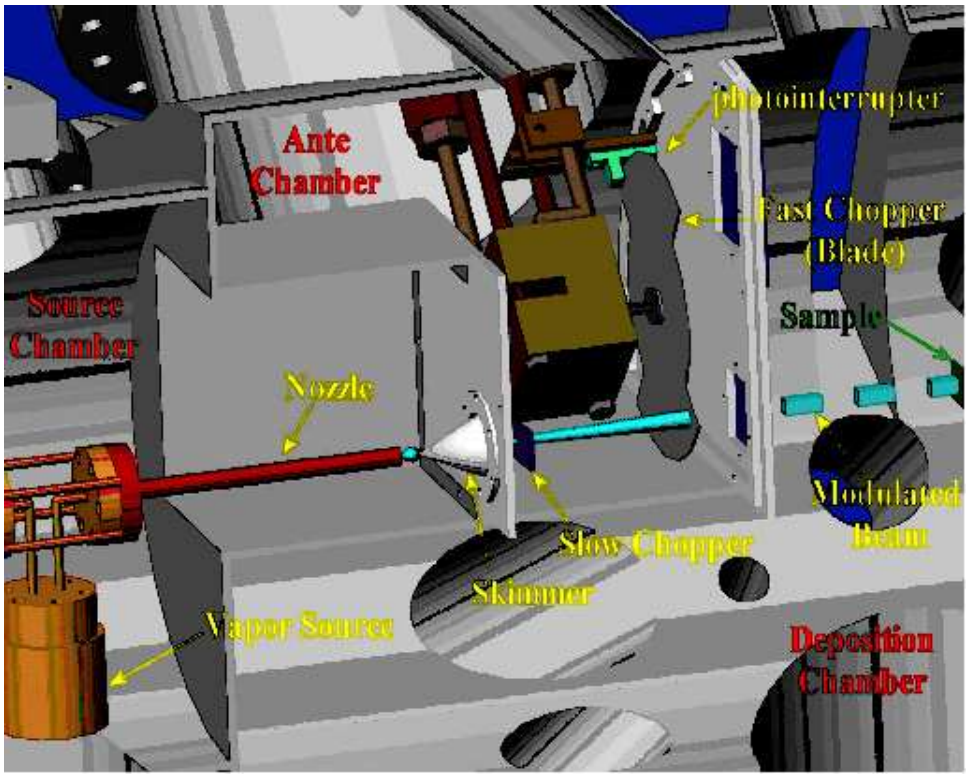

Figure 3.3: Illustration of the collimated molecular beam in the supersonic molecular beam chamber at G-line [11].

the sample. The window placed at the incoming flight path of the x-rays is placed horizontally, while the one on the outgoing flight path is placed vertically. This allows synchrotron x-rays to enter the chamber from varying angles and after scattering from the sample the x-rays pass through the second vertically positioned Be window, where they are detected by a x-ray detector mounted on a Huber stage. The schematics of the top view of the supersonic chamber with the x-ray positions are shown in Figure 3.4. The system is mounted on the diffractometer table and the motion of the table allows for the precise manipulation of the UHV chamber with respect to the incoming flight path of the x-rays. The rotation of the sample holder in the plane defined by the entering x-rays (theta, motor name ”th”) and about the surface normal (zeta) can be used to do various scans and real time experiments. To do the anti-bragg scans, the intensity of

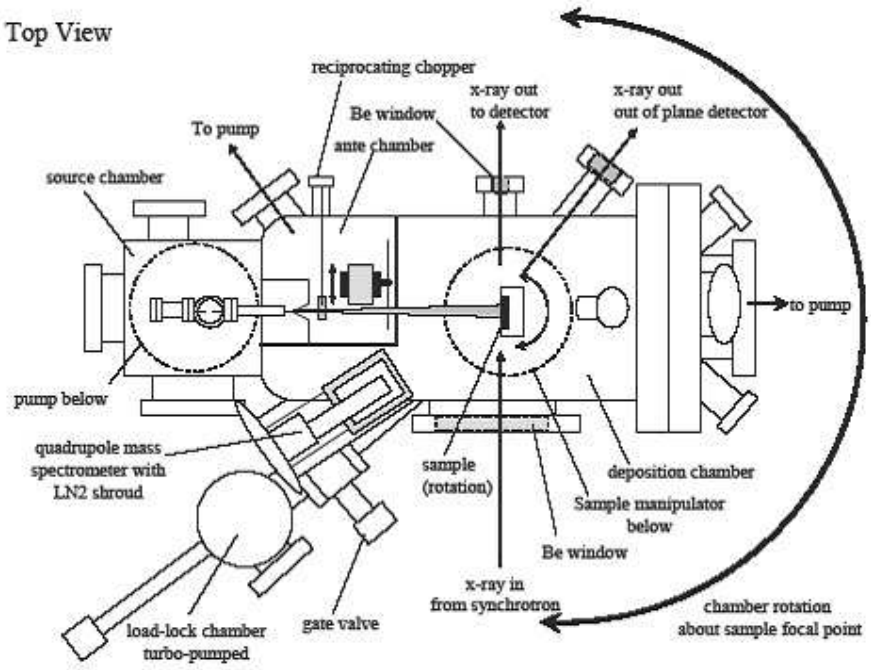

Figure 3.4: Top view of gas deposition source system (G-line) [11].

the scattered x-rays from the sample is monitored at the grazing incidence position. This helps in analyzing the growth modes and film quality. In-plane measurements help in determining the crystal texture while out of plane measurements determine crystal structure and quality.

The load lock carries a transfer arm and is used to mount the sample holder without having to vent the entire chamber. The load lock is pumped by 300 Ls^{-1} turbo pump (Seiko, STPH 300C), and reaches a base pressure of 5 x 10^{-7} Torr within a couple of hours of mounting the sample. The load lock and the main chamber are separated by a gate valve and the sample is transferred by a magnetically coupled linear rotary feedthrough with a STLC (thermionics) type transfer system. Through a set of clips, the platen can be locked or unlocked on the manipulator or the transfer arm. Usually sample dimensions vary from 1 cm x 1 cm to 1.5 cm x 2 cm, depending on the type of

experiment. Samples sit in recessed wells in those platens and are held in place by a retaining ring and three clips on the sample holder.

The substrate holder can be heated or cooled to temperatures as high as 90°C or as low as -60°C. The platen exposes the back of the sample to facilitate radiative heating and retaining rings help minimize thermal stresses incurred during heating. Sample surface temperatures can be measured be measured using a K type thermocouple. A K type thermocouple is also mounted on the back of the manipulator and is calibrated to temperature measurements at the surface of the sample. To go to a temperature as low as -60°C, liquid nitrogen is used as the circulating fluid around the manipulator. The manipulator is capable of two rotational degrees of freedom (θ, azimuthal), and is pumped by a differential sealed rotary pump. The sample holder is fitted with a radiant graphite heater, capable of heating Si samples. It can be cooled to a temperature as low as 170K by providing contact through copper braids to a liquid nitrogen cooled reservoir. A thermocouple is attached to the Mo platen to read the temperature of the sample directly. A reference thermocouple is attached at the back of the manipulator and is used for temperature calibration. A quadrupole mass spectrometer (Extrel EX-800) can also be mounted in a direct line of sight at the end of the main chamber. The ionizing region of the mass spectrometer is surrounded by the liquid nitrogen shroud.

The supersonic molecular beam chamber has two chopper blades. One is the reciprocating flag (slow chopper), which modulates the beam from the skimmer before entering the antechamber, and is used to define exposures of the samples to the molecular beam. Other is the rotating blade chopper (fast chopper), which can be employed to produce fast molecular beam waveforms and can be used to do some time of flight measurements with a quadrupole mass spectrometer. The blade chopper is mounted on a linear translational stage.

3.1.1 Sample Preparation and Handling

Substrates used to grow films for growth experiments are Si (100) wafers (Wacker-Siltronic, p-type, 4" dia., 500-550 μm thick, 38-63 ω-cm). To grow a 300 nm thick film of thermal oxide, the wafers are first treated with RCA-1 clean, HF dip for 15 sec, followed by RCA-2 clean immediately before growing SiO_2. The thick SiO_2 films are then grown by wet thermal oxidation at 1100°C for 19 min at the thermal oxide furnace at Cornell Nanoscale Science and Technology Facility (CNF). These wafers were then cleaved in small samples of 1.5 cm x 2 cm to do growth experiments at various conditions. Highly doped n or p-type wafers after subjected to above steps were used to deposit films used to make thin film transistors.

Thermal oxide clean

The objective of the thermal oxide clean of the wafers is to remove any macroscopic particles and organic matter, sticking to the surface. The clean is done immediately before placing the sample in the loadlock of the vacuum chamber. The wafers are first placed in anhydrous chloroform ($CHCl_3$) solution (99%) and were wiped clean with a swab. They are then sonicated in the $CHCl_3$ solution for about 15 min. After sonication in $CHCl_3$, they are allowed to air dry and then sonicated in deionized water. They are then washed with deionized water and dried with nitrogen. After drying, the samples are placed in ultraviolet light-ozone (UV-Ozone) cleaner for 10 min. The samples should be placed in the loadlock within 15 min of the UV-Ozone clean.

Hexamethyldisilazane(HMDS) coating:

After the cleaning process, the surface can be coated with HMDS. Samples are placed in YES LP-III vapor priming oven at CNF. The substrate is held at 150°C and HMDS is deposited in vapor phase after successive evacuation and purge cycles used to dehydrate

the substrate. The entire process lasts for 25 min and the vapor pressure is 6 torr. The samples should be placed in the loadlock within 15 min after removing from the oven.

3.2 G-Line Setup

3.2.1 Description of G-line Setup

The experiments involving in-situ analysis of organic thin films using x-ray diffraction was carried out at G-3 hutch at G-line in Cornell High Energy Synchrotron Source (CHESS). G-line has three stations called as G-1, G-2 and G-3 hutches. The rotating positron beam produces x-ray radiations that feed all the hutches in G-line. The x-ray beam coming from the synchrotron source is split into two sections in G-cave by a pair of multilayer monochromators. One part of the beam enters the G-1 hutch while the remaining section passes through a pipe to enter the G-2 hutch. A part of the beam is deflected to enter G-2 and the remaining part enters the G-3 hutch to be used for in-situ growth analysis of films grown by PLD and SSMBD. The high intensity beams (8-12 keV) have been used for a wide variety of research. G-1 diffractometer has been used for time resolved studies using small angle x-ray scattering (SAXS), G-2 hutch has a high resolution diffractometer that is used for in-depth analysis of the structure and growth dynamics of the films. G-3 hutch is customized for the in-situ analysis of growth dynamics of organic and inorganic thin films grown by SSMBD and PLD.

3.2.2 G-3 Diffractometer

The G-3 hutch has a diffractometer which has been used for in-situ growth analysis of organic and inorganic thin films growth by SSMBD and PLD respectively. It has various stepper motors which govern the motion of the diffractometer table and the incoming

and outgoing flight path. The motion of the incoming flight path is controlled by four motors: yeast, ywest, zeast and zwest. Yeast and ywest control the horiztonal motion while zeast and zwest control the vertical motion. For alignment procedures yeast and ywest should be moved together to avoid damage to the incoming flight path, and so is the case with the zeast and zwest. The diffractometer table has motors called as zsouth (zs), znortheast (zne) and znorthwest (znw) which control the vertical motion of the diffractometer table. The y motor of the diffractometer control the horizontal motion of the diffractometer table.

3.2.3 Supersonic Molecular Beam Chamber at G-3

The incoming flight path has two slits called as S1 and S2 and three ion chambers called as I0, I1 and I2. The S1 slit is present between I0 and I1 while the slit S2 is present between I1 and I2. The sizes of the slits can be adjusted to produce a narrow beam using screws on the sides. The beam leaving the ion chamber I2 enters the Beryllium (Be) window mounted on the chamber. The beam then strikes the sample where pentacene is being deposited continuously on the Si wafer. The diffracted beam exits from another Beryllium window placed close to the outgoing flight path. The exiting flight path has another ion chamber called as I3 which measures the intensity of the beam going in the detector (Bicron or Bede). The oscillations of the diffracted intensity are recorded as a function of time and are used for further analysis.

3.3 Grazing Incidence Wide Angle x-ray Diffraction (D-line Setup)

One of the other techniques that have been used for the analysis of pentacene thin films is grazing incidence wide angle x-ray diffraction (GIWAXS). The ex-situ analysis using WAXS was carried at D-line at CHESS. The D-line set up consists of an incoming flight

path with slits, followed by a beamstop and a CCD detector. The samples to be analysed are placed at the top of the beamstop. Wide angle x-ray scattering is widely used for analysis of films where the Bragg peaks are scattered to wide angles. In this we reduce the distance between the sample and the detector so that Bragg peaks at large angles can be analyzed to determine the crystal structure.

3.4 Molecular Beam and x-ray alignment

The alignment of the x-ray beam forms the very first and the most significant step during any experimental run. The G-line x-ray optics provides an ultra high x-ray flux for scattering experiments. The very first challenge is to align the x-rays with the molecular beam and make them hit the center of the sample. The alignment is an important step because the x-ray beam position could wander in response to changes in the x-ray optics. The chamber (mounted on the diffractometer table) can be rotated by using various motors (zs, zneast, znwest and y). The sample holder can be rotated in the plane and perpendicular to the axis of the x-ray beam. To accommodate the changing position of the beam the optical table is translated so that the diffractometer rotational axis intercepts the beam axis. Through this the samples can be roughly lined up. SPEC software package is used to more accurately position the samples which integrates the total intensity under a set of characteristic lines as the sample is translated through the beam. For the same incident angles chamber translation was in y-direction. This motion is called as chamy. The intensity can thus be plotted (counts obtained at the detector) as a function of chamy and the chamber is moved to the maximum intensity. With chamy being set at the maximum the angle θ (between the sample and the x-ray beam) is set. First, the 2θ angle of the x-ray detector for a given scattering geometry is set. The table rotation angle which, sets the angle between the sample surface and the incident x-ray beam, is called μ and the rotation angle of the detector arm is called γ. The angle 2θ (between the

incident x-ray beam and the detector) equals the sum of μ and γ. But μ being dependent on the surface, only one value of μ (and hence γ) allows specularly reflected x-rays to enter the detector. The angle is μ is rocked over a narrow angular range to find a unique value. The value is set to where we obtain the maximum intensity. While rocking μ, γ is simultaneously rotated, to maintain a constant value of 2θ. After obtaining the right values of μ and γ, chamy scans are repeated using the specular beam as a guide. This completes the lineup procedure.

Chapter 4
Sample Characterization

Sample characterization is important to analyze the growth of thin films. Various ex-situ techniques such as atomic force microscopy, scanning electron microscope and in-situ techniques such as x-ray diffraction have been used to understand the dynamics of thin films growth for device applications.

4.1 In-situ analysis techniques

In-situ analysis techniques such as x-ray diffraction have been widely for analyzing both organic and inorganic films grown by thermal and supersonic deposition methods

4.1.1 X-ray diffraction

X-ray diffraction has been a widely used for the in-situ analysis of thin films grown by various deposition methods. More about x-ray diffraction has been discussed in chapter 1.

4.2 Ex-situ analysis techniques

Following film deposition and in-situ analysis by X-ray diffraction, ex-situ analysis was performed using Atomic Force Microscopy and Grazing Incidence Wide Angle X-ray Diffraction (GIWAXS).

4.2.1 Atomic Force Microscopy

Atomic Force Microscopy (AFM) is a widely used ex-situ analysis tool which helps in understanding the thin film morphology at a nanometer scale. After the removal of the

sample from the vacuum chamber, the samples are analyzed using a Digital Instruments Dimension 3100 scanning probe microscope (Veeco Instruments) in tapping mode. The images were obtained at three different scales: 2*mu*m x 2*mu*m, 5*mu*m x 5*mu*m and 20*mu*m x 20*mu*m. Using the Nanoscope software (v 5.0) the images were fitted to obtain a correlation between the roughness and the specific surface features. These correlations are described in the form of power spectral density (PSD). PSD is defined as the square of the magnitude of the coefficients of the Fourier Transform of a digitized surface. The transformation is called 1DPSD when it is carried out in one direction. 1DPSD, at a particular frequency (f),is given by the following formula:

$$PSD(f) = \frac{1}{L} \mid \int_0^L dx h(x) e^{i2\pi f x} \mid^2 \tag{4.1}$$

Here h(x) is the line profile in the scan direction, x and L is the scan length. 1DPSD analysis can be further used to characterize the surface morphology and calculate the roughness and the scaling exponents. Since 1DPSD analysis provides a relation between the PSD power (magnitude) and the spatial frequency (inverse of the lateral length scale), the analysis gives correlation between the roughness and the spacing between the various surface features like mounds, islands etc. Based on the PSD analysis, one can figure out roughness scaling exponents α which is related to γ as

$$\alpha = \frac{\gamma - d}{2} \tag{4.2}$$

where d is the line scale dimension and is equal to 1 for 1D-PSD. All AFM images were obtained for three different scan sizes and 1D-PSD was performed for the scan size of 20 x 20 μm^2. Along the scan direction, one dimensional PSD were calculated and single line PSD(s) were averaged.

4.2.2 Grazing Incidence Wide Angle X-ray Diffraction (GIWAXS)

The orientation of the molecular thin films plays a very significant role in defining the morphology and structure of the thin films and its application in organic electronic for making photo voltaic devices, light emitting diodes etc. Wide Angle X-ray scattering provides a huge amount of information about the film structure that might be hidden in AFM, and hence has been used for the ex-situ analysis of the films grown under vacuum in the UHV chamber at G3 hutch at CHESS. Molecules such as pentacene show a pronounced polymorphism when grown under different growth conditions. Grazing Incidence Diffraction is a powerful tool used to study thin film structure of such molecules. Its combination with wide angle scattering is advantageous for organic thin films so as to prevent damage to the films as the X-ray intensity is spread over a large scattering area. GIWAXS measurements have been carried at the D1 hutch at CHESS. The samples are placed on a beamstop (D1 setup), and the x-rays diffract to give a multitude of Bragg peaks which can be observed on one pixel space map. The images are obtained using the fit2D software. These can then be converted into reciprocal space to obtain the lattice parameters [(Smilgies et.al (2007))]. These help in indexing the peaks and observe if any new polymorphs are being formed for a specific growth condition - as for the case of films grown at extremely high growth rate of 2 ML.s^{-1}.

Chapter 5
In-situ X-ray scattering of pentacene thin films

5.1 Overview

Pentacene has been widely studied as a prospective organic molecule for growing thin films which can be used for making organic thin film devices. However the orientation of the molecules plays a very significant role in defining the morphology and the structure of the films. Growth conditions like growth rate, kinetic energy of the incident beam, temperature of the substrate form an important controlling factor for the texture of the film, shape of the islands etc.. Hence it is very important to identify the parameter space that can be used to grow smooth films which can be further used to grow devices. Growth experiments with pentacene seeded in Helium have been carried in UHV supersonic molecular beam chamber at G3 hutch in CHESS under various growth conditions:

1. Varying the growth rate (GR) from 0.008 ML-s^{-1} to 2 ML-s^{-1}
2. Varying the substrate temperature (Ts) from 90°C to -60°C
3. Varying the kinetic energy of the beam from 2.7eV to 6.7eV
4. Varying the substrate - carrying growth experiments on precleaned Si wafers with native oxide deposition and with HMDS coating on the surface.

5.2 Supersonic molecular beam deposition of pentacene under different growth conditions

Pentacene has been traditionally deposited by thermal evaporation on amorphous SiO_2, and its growth has been studied by ex-situ atomic force microscopy (AFM) and X-ray

diffraction [33]. Supersonic molecular beam deposition has recently emerged as a powerful technique that provides an edge over thermal evaporation. It has recently demonstrated to provide a spatially well defined, directed and collision free flux of molecules combined with well controlled kinetic energy in hyperthermal range (1eV up to 13eV). Another advantage of using supersonic molecular beam deposition lies in the fact that it allows full control of the flux and the beam direction and it decouples the energy of the arriving molecules from the thermal energy of the substrate [45, 46] thus producing a very stable and uniform beam with excellent control over its kinetic energy and flux. While the effects of incident kinetic energy and substrate atomic structure have been examined in other hyperthermal systems (plasma assisted and ion-assisted deposition), similar work is very much lacking on organic semiconductors grown by supersonic molecular beam deposition [47]. The following chapter describes the growth experiments carried out in various experimental conditions like varying incident kinetic energy, varying growth rates, different substrate temperatures and different substrates. There exists a strong correlation between physical and electronic properties of thin films of organic materials with the choice of substrate and deposition conditions which has been shown by recent studies [48]. The analysis is done in-situ using anti-bragg scattering and grazing incidence diffraction and further insight is given by the ex-situ analysis using atomic force microscopy.

5.2.1 Growth rate series of pentacene on SiO_2

Pentacene is a promising molecule for organic thin film applications. It has been reported previously that deposition rate along with other factors have a great significance on the crystalline grain size of pentacene thin films [49]. Gundlach and co-workers reported that pentacene films deposited at low to moderate deposition rates have a better degree of molecular ordering and yield thin film transistors (TFT's) with higher mo-

bility [22]. Pratontep and co-workers studied the effect of growth rate and substrate temperature on pentacene thin films on SiO_2 substrate deposited under high vacuum conditions using ex-situ atomic force microscope in tapping mode. They found that the number density of the islands increase by a similar factor as the deposition rate and the reverse is observed with increasing substrate temperature [50]. These two parameters, growth rate and substrate temperature can thus be tuned to control the density of grain boundaries of pentacene molecules on SiO_2 and hence the charge transport properties in organic field effect transistor devices. Yanagisawa and co-workers studied the effect of deposition rate and substrate temperature on the mobility of pentacene thin film transistors (TFT's). They found that even under different growth rate and substrate temperature conditions the films were mainly composed of thin film phase and different orientation of the grains is a major hindrance for obtaining good mobility [51]. Lin and co-workers reported in an IEEE publication the effect of substrate temperature and deposition rate on field effect mobilities on pentacene TFTs. They reported mobilities larger than $0.2cm^2V^{-1}s^{-1}$ at a temperature of 20 to 150°C and at a deposition rate of 2 to 8 Å/s [52]. Knipp and co-workers observed the effect of deposition rate on pentacene films grown on SiO_2 using x-ray diffraction. They found that as the deposition rate is reduced, the size of the dendrites reduces, however the ratio of the diffraction peaks remain unchanged [53].

Pentacene, a promising organic semiconductor [1, 54], is known to form highly ordered thin films with charge carrier mobilities reported as high as $1.5cm^2V^{-1}s^{-1}$ [52] exceeding that of amorphous silicon ($1\ cm^2V^{-1}s^{-1}$). In this chapter fundamental phenomena and principles involved in ultra high vacuum deposition of thin films using supersonic molecular beam has been discussed. The first parameter to take into account is the deposition rate. Apparatus and experimental details have been described in section 3.1. However, a brief description is mentioned below. Thin film deposition has been

carried in ultra high vacuum chamber [46].The base pressure of the chamber prior to deposition was 2 x 10-9 torr. Substrates (4" Silicon (100) wafers) were subjected to an RCA-1 clean, 15 sec HF dip followed by an immediate RCA-2 clean before the growth of 300nm thick film of SiO_2. The 4" wafers were then cut into small samples of sizes 10mm x 10mm. These small samples were then cleaned and degreased by sonication for 15 min in anhydrous chloroform solution (99% $CHCl_3$) and 15 min sonication in DI water. They were then dried with N2 and cleaned with UV-Ozone for 10 min. The sample was immediately loaded in the load lock. Supersonic molecular beams of pentacene (99.8% Sigma-Aldrich) were generated by flowing a carrier gas (Helium 99.999% Air Gas) over a temperature controlled container of pentacene (the bubbler / evaporator) which is located upstream of the nozzle. The growth rate can be controlled by tuning the temperature of the bubbler, as that determines the amount of pentacene being evaporated and added to the carrier gas. The flow of the carrier gas can be modulated using a mass flow controller (MKS). The depositions were carried out by varying the bubbler temperature from $223^{\circ}C$ to $320^{\circ}C$, which correspond to a deposition rate of 0.08ML-s^{-1} to 2ML-s^{-1}. The heatable nozzle consists of 0.25" diameter stainless steel tubing which has a 125μm stainless steel plate at the end with a 150μm orifice machined into it. The doubly differentiated pumped beams pass through a trumpet shaped skimmer (2.0mm aperture, Beam Dynamics) into an antechamber. The aperture plate was removed for the first set of experiments so as to center the molecular beam spot and to avoid any scattering from the substrate surface. The beams were blocked using a shutter in the antechamber which facilitated precise exposure of the substrate to the beam. This was necessary to ensure that all the films grown were of a constant thickness. In-situ analysis was done using grazing incidence diffraction and anti-bragg scattering. The X-ray data thus obtained was fitted to the modified Cohen model and various parameters were obtained to understand the growth phenomena. Following the removal of the sample from

the chamber, the samples were analyzed using a Digital Instruments Dimension 3100 microscope (Veeco Instruments) in tapping mode. AFM images of different dimensions were obtained: 2 x 2μm2, 5 x 5μm2 and 20 x 20μm2. One dimensional PSD spectra (1DPSD) was used to characterize the roughness and to obtain the correlation lengths to understand the island size distribution. The analysis of the data obtained has been discussed in detail in chapter 6.

5.2.2 Effect of energy and substrate on pentacene growth

Deposition of pentacene on two different substrates - SiO_2 and HMDS, incident at hyperthermal energies ranging from 2.7 eV to 6.7 eV, has been investigated with in-situ grazing incidence diffraction and anti-bragg scattering. Ex-situ analysis has been done using atomic force microscopy in tapping mode. Semiconducting organic materials have been a constant focus of research activity because of their potential application in electronic and optoelectronic applications - organic field effect transistors, organic light emitting diodes and organic solar cells [54–56]. Film growth and the resulting morphology is typically a surface phenomenon mediated by kinetic energy as has been seen in both inorganic [57, 58] and organic film growth [10, 59, 60]. As discussed above the morphology of pentacene thin films depend upon the growth conditions like substrate temperature, incident kinetic energy, substrate modifications and growth rate. The effect of growth rate has been discussed in brief in the previous section and will be dealt more in chapter 6.

In this section we discuss the effect of incident kinetic energy and the substrate composition on growth mode and film morphology. Incident kinetic energy of molecular beam affect the sticking and adsorption probability, thus affecting nucleation, island formation, crystallization and steady state film growth. Incident kinetic energy along with other deposition parameters like substrate temperature, deposition rate affects the

diffusion timescales, which in turn affect the shape of growing pentacene islands. Because of this difference in diffusion time scales (surface movement versus hopping on the step edge), a fractal shape is often observed for growing islands [48, 61]. It has been found that pentacene films deposited by pulsed laser deposition are smoother and have enhanced electrical properties than the films deposited using thermal evaporation [62]. It has been shown that pentacene films deposited on single crystal Ag employing high incident kinetic energy supersonic molecular beams have increased order (as measured by X-ray reflectivity) that the films deposited with incident energy close to thermal energy [47]. Supersonic molecular beams provide a great potential to tune the incident kinetic energy of pentacene molecules which strongly influence the film morphology. Few studies in the past on thin film morphology reveal this fact as well. Casalis and co-workers observed the growth of pentacene on Ag (111) at 200K and hyperthermal energies of the range of 5 eV. Using in-situ low energy atomic diffraction (LEAD) they found that the pentacene molecules grow in a layer by layer fashion and highly ordered films are formed. They attributed this effect to the local annealing induced by the impact of the hyperthermal molecules at a low substrate temperature [47]. Iannotta and co-workers [14] observed the growth of pentacene films with incident kinetic energy varying from 0.3eV to 5.5eV. They analyzed the films with atomic force microscope and found that the grain size for the films grown at 0.3eV is much smaller (100 - 200 nm), whereas the films grown at 5.5eV had ordered pentacene crystallites larger than 1 - 2μm. The film grown at 5.5eV was reported to show mobilities of $0.5 cm^2 V^{-1} s^{-1}$ [31]. Killampali and co-workers also observed the effect on the nucleation of pentacene on silicon dioxide at hyperthermal energies. They found that the incident kinetic energy strongly influences the process of adsorption and hence the deposition rate but it doesn't affect the nucleation process to a great extent. As the incident kinetic energy is increased from 1.5 to 6.7 eV the deposition rate decreases from 1.5 to 0.5 ML-min^{-1} [32].

Since pentacene is one of the most widely studied organic semiconductors for thin film transistors, efforts have been made to understand its growth on various substrates other than SiO_2. The choice of the substrate drastically affects the mode of the growth. Heringdorf and co-workers observed that the pentacene films, when grown on SiO_2 show a high nucleation density and forms small islands consisting of vertically oriented molecules. However when they were grown on Si(001) the nucleation density of the thin films phase is much smaller and it develops on the top of the wetting layer formed by the pentacene films. The adsorption of cyclohexene SAM prevents the formation of the wetting layer. They found that the even though the substrate determines the diffusion length of the molecules, the interaction between the molecules on the surface governs the critical size of the islands [63]. Oehzelt and co-workers investigated the growth and morphology of pentacene thin films on polycrystalline copper surfaces grown by vapor deposition in ultra high vacuum conditions at different substrate temperatures. They found that the change in the substrate temperature has a strong influence on the size of the crystallites. The long range order is missing when the films are grown at 77K than at 333K, and the growth is not completely epitaxial. There exists several crystalline phases when films are grown on polycrystalline substrates, and this can be controlled by tuning various deposition parameters and substrate quality [64]. Spence and Wu studied the structure of pentacene thin films on NaCl substrates by electron diffraction and found the existence of a new thin film phase with d spacing of 15.1 Å [37]. Fritz et.al studied pentacene films deposited on amorphous SiO_2 (a-SiO_2) and found that the pentacene monolayer deposited on a-SiO_2 is highly crystalline and has a structure differing from (001) layers in single crystals of bulk pentacene [23]. The structure was more similar to pentacene multilayer formed on (100) NaCl substrate by Wu and Spence [37]. Koo and co-workers reported the effect of substrate treatment using HMDS on the morphology of pentacene films and found that the thin film transistors formed on pentacene

deposited on HMDS showed higher mobilities as compared to ones formed on a-SiO_2 and hence better performance [65]. Studies on pentacene growth on substrate modified with hexamethyldisilane (HMDS) showed that the probability of trapping a molecule is higher on the surface modified with HMDS, and the island density is much larger (with the island formed being two molecules high) on HMDS than the films deposited on SiO_2 [26]. Films grown on substrates modified with HMDS are known to roughen slowly and hence show organic thin film transistors (OTFTs) fabricated from pentacene deposited on SiO_2 modified with HMDS show a better performance characteristics than the films deposited on bare SiO_2. Ruiz and co-workers reported the growth of pentacene on Ag(111) at 200K as diffusion mediated with the critical island size of four molecules [27,66]. Richter and co-workers found using X-ray reflectivity during the formation of octadecyltrichlorosilane (OTS) monolayers on Si(111) surface that the films undergo island type growth [67]. Fanetti and co-workers reported through scanning tunneling microscope (STM) formation of rippled morphology of pentacene molecules on copper (119) surface. They also reported that a long range order can be obtained by the thermal treatment of thick films of pentacene [68]. Park and co-workers reported the transition from 2D to 3D at room temperature when the deposition of perylene was carried on SiO_2 modified with octadecyltrichlorosilane (OTS) [69]. There has been continuous work going that shows the effect of varying incident kinetic energy and substrate modifications on the grain size, morphology and texture of thin films. An effort has been made to understand the impact of these parameters on pentacene films grown by supersonic molecular beams in UHV conditions through in-situ x-ray diffraction and ex-situ atomic force microscope (AFM).

The apparatus and the chamber description have been described in the experimental section. The energy of the helium beam in which the pentacene molecules are seeded can be controlled and changed using the MKS controller mounted on the electronics

rack. Analysis of the samples was done in-situ using X-ray diffraction and ex-situ by atomic force microscope (AFM). The intensity versus time data thus obtained was fitted to a modified Cohen model. The various fitting parameters described in the results and analysis section gives a deeper insight into the effect of kinetic energy and substrate modifications on thin film morphology.

5.3 Analysis and Results

Surface engineering for e.g. modification of surface termination using self assembled monolayers is known to significantly affect transport properties of small organic molecules. Pentacene was deposited on two different substrates, SiO_2 and HMDS deposited on SiO_2. The growth was monitored using in-situ anti-bragg scattering and ex-situ using atomic force microscopy. The results along with the cohen model fits are shown in Figure 5.1 and Figure 5.2. For the film grown on SiO_2, we observe that A1¿A2, which indicates that the first layers completes before the formation of the second layer begins. This is in confirmation with the cusp in the intensity oscillations for pentacene grown on SiO_2. For pentacene on HMDS-modified SiO_2, we observe that surface modification influences the adsorption probability of the molecules on the surface as A1¡A2. However from the layer coverage it is evident that the first layer is complete before the second layer starts to grow. In the case of growth on HMDS-modified SiO_2, it is clear that the first two layers grow completely as shown by the layer coverages. It is evident that surface termination affects the formation of crystallites and hence their nucleation and growth behavior thus affecting film morphology.

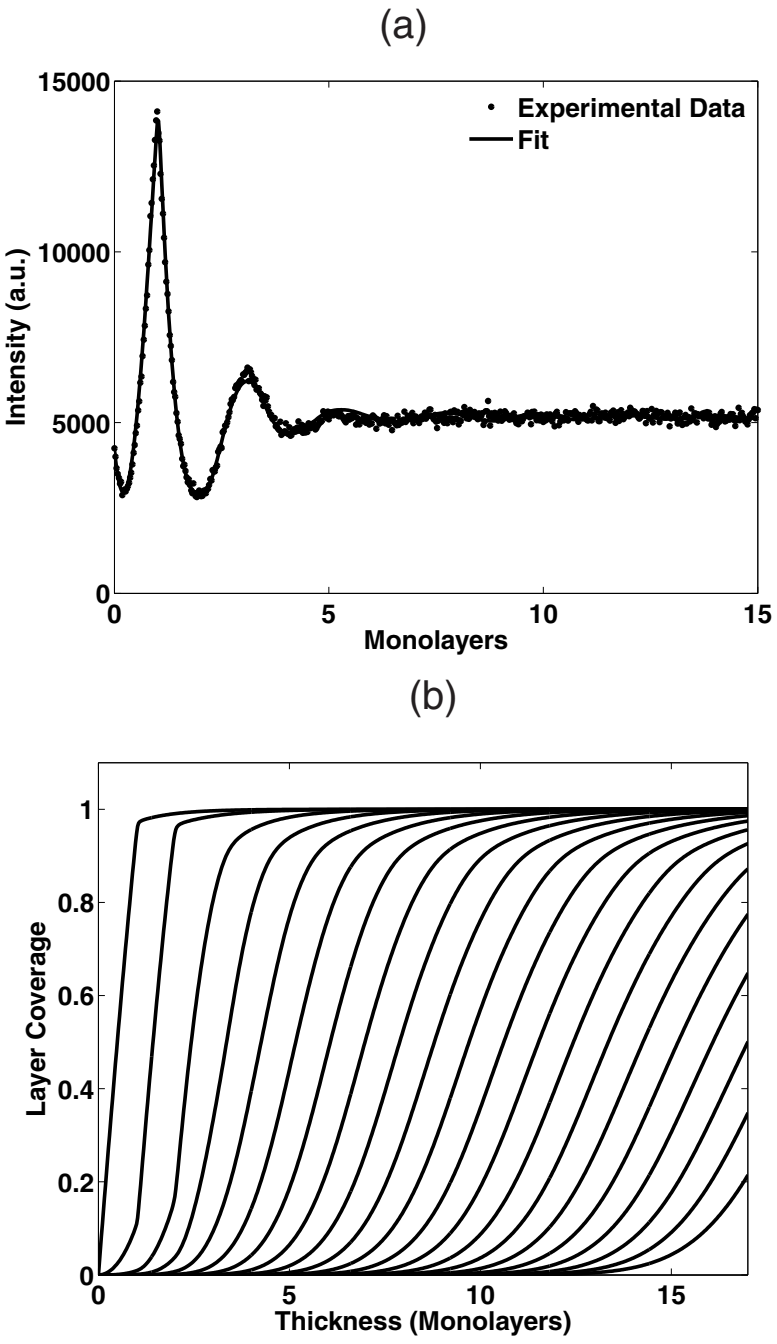

Figure 5.1: (a) Intensity oscillations for pentacene grown on SiO_2 at 30°C at 4.6 eV (b) Layer coverage for pentacene grown on SiO_2 at 30°C at 4.6 eV.

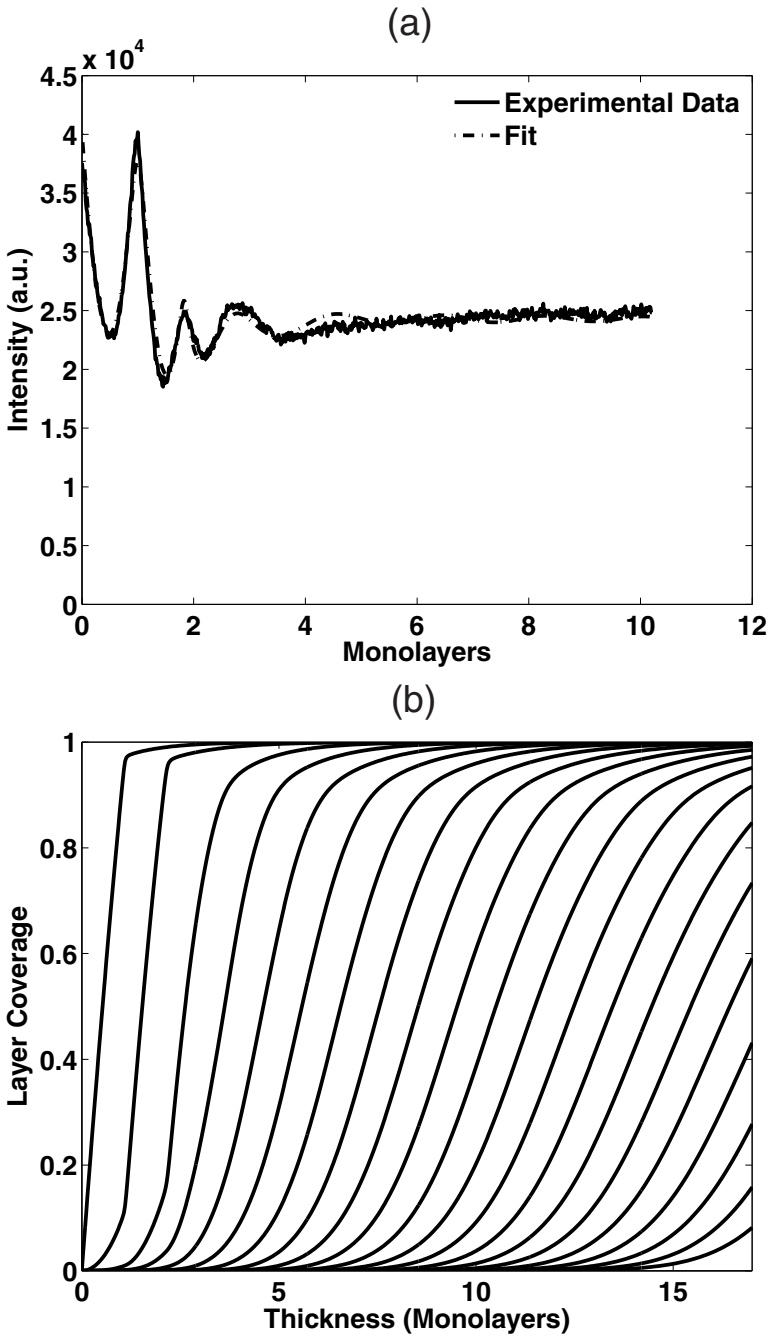

Figure 5.2: (a) Intensity oscillations for pentacene grown on HMDS at 30°C at 4.6 eV (b) Layer coverage for pentacene grown on HMDS at 30°C at 4.6 eV.

5.3.1 Effect of substrate temperature on pentacene thin films

Substrate temperature is a very important factor that influences the morphology of the film to a great extent. The mode of the film growth (2D, layer by layer, 3D) of the films depend on growth conditions (substrate temperature being one of those) and also on the interaction strengths between the adatoms/admolecules diffusing on the substrate and the substrate. Burton, Cabera and Frank reported that there exists a thermodynamic driving force (defined as the positive difference between the chemical potential of a molecule in vapor and crystal phase) which determines the kinetic rates of the processes such as impingement, sticking probability of the adatom to the substrate, surface diffusion, desorption, nucleation and coalescence, hence it has a significant impact on the shape of the islands. Growth conditions such as deposition rate, substrate temperature significantly affect these kinetic rates and hence the processes [70]. It has been reported that the number of stable nuclei formed during nucleation are a strong function of substrate temperature [71, 72]. Zuppiroli and co-workers examined the nucleation of pentacene on SiO_2 by ex-situ atomic force microscope (AFM) and found that the island density increases with deposition rate and decreases with substrate temperature, consistent with homogeneous nucleation and growth via capture of diffusing admolecules [50, 73]. Sanvitto and co-workers studied the deposition of C_{60} on H-Si(100). On increasing the substrate temperature they found a transition from 2D at room temperature to 3D at 473K [74] and a similar transition was reported by Mobus and Karl for PTCDA deposited on Si at elevated temperatures [75]. Biscarini and co-workers studied the effect of substrate temperature on sexithienyl films deposited by evaporation on freshly cleaved mica substrates in high vacuum using atomic force microscopy (AFM) in contact mode [76]. They found that the films grown at a temperature $< 200^{\circ}C$ were granular and growth was diffusion mediated. They also reported in another paper the effect of substrate temperatures $> 200^{\circ}C$ using AFM in contact mode and found that the

film morphology is lamellar and the deposition is more controlled by adsorption [77]. Pentacene films deposited on quartz substrates were studied using optical absorption spectra and were found that the films deposited below -90°C were amorphous. This was also examined by another group using x-ray diffraction which deposited pentacene films on quartz substrates at -50°C and 10 Å/s and found that the pentacene films grown in these conditions were amorphous [78, 79]. Lee and Kim reported that the pentacene crystal structure changes with when pentacene films were deposited on Al_2O_{3+x} layer and as the substrate temperature was varied. They found that as the substrate temperature was increased from room temperature to 90°C bulk phase dominates [80]. Salih and co-workers studied pentacene films deposited by thermal evaporation and pulsed laser deposition (PLD) and found through AFM that the films deposited by PLD were smoother and gave better mobilities. They also reported that films deposited by thermal evaporation at higher substrate temperatures showed the presence of larger crystallites, increased molecular ordering, higher film densities and increased mobilities [62]. Pratontep and co-workers reported the effect of deposition rate and substrate temperature on pentacene films deposited on SiO_2 and found that the nucleation density of the islands increases on increasing the deposition rate but decreases at higher substrate temperatures. Through selected area electron diffraction (SAED) they determined the formation of a bulk triclinic phase at a substrate temperature of 80°C [50]. Gundlach and coworkers determined a higher degree of molecular ordering, large dendritic grains and TFT's with higher mobilities in pentacene films deposited at elevated temperatures [22].

Pentacene films were deposited in supersonic molecular beam chamber in UHV conditions, described elsewhere. The substrate holder (on which the substrate is mounted) can be heated or cooled with the help of eurotherm (to increase temperature) and liquid nitrogen (to decrease temperature below 0°C) respectively. The temperature of the platen on which the substrate is mounted is the reference temperature. The actual sub-

strate temperature can be calibrated with regards to the reference temperature. There are two thermocouples, one is placed in contact with the substrate with the help of the clips on the substrate holder to give an accurate reading of the substrate temperature, and other is placed at the back of the substrate holder which measures the substrate temperature. Experiments are carried where pentacene is deposited in UHV conditions with substrate temperatures (T_s) varying from -65°C to 90°C. In-situ analysis is done using grazing incidence diffraction and ex-situ analysis is done by AFM and X-ray reflectivity measurements at G2 hutch at CHESS. The following section describes the results and the analysis based on the parameters obtained from fitting the modified Cohen model to the intensity versus time data obtained from in-situ grazing incidence diffraction.

Analysis and Results

Substrate temperature, as discussed above, is known to affect the film morphology to a significant extent. In Figure 5.3, 5.4 and 5.5 we represent the real time anti-bragg scattering data obtained for pentacene grown on SiO_2 at room temperature (30°C), -17°C and -66°C at 2.7eV and 0.13 ML-s^{-1} respectively. From the AFM images (Figure 5.6), it is clear that the films become amorphous as the substrate temperature is reduced. It is clear that as the temperature is decreased, the intensity oscillations damp much rapidly. At a substrate temperature of -66°C, we don't observe one complete oscillation. The AFM clearly shows the existence of a cauliflower like morphology at the lowest temperature of -66°C while a distinct terraced 3D morphology is observed for the film grown at room temperature. The ex-situ x-ray reflectivity measurements show the existence of the thin film phase over the entire temperature range from room temperature to -66°C to 30°C. There is no evidence of any structural changes or bimodal growth.

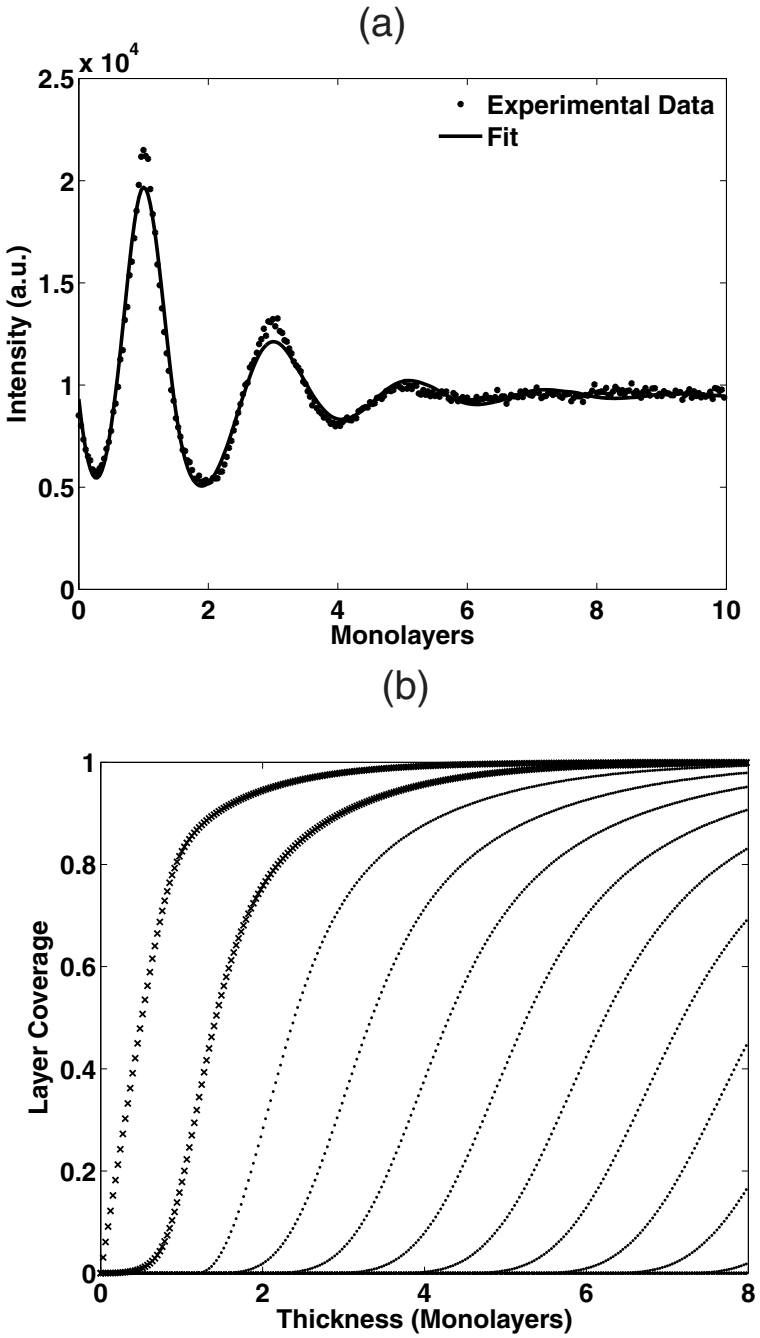

Figure 5.3: (a) Intensity oscillations for pentacene grown on SiO_2 at room temperature (b) Layer coverage for pentacene grown on SiO_2 at 30°C at 2.6 eV.

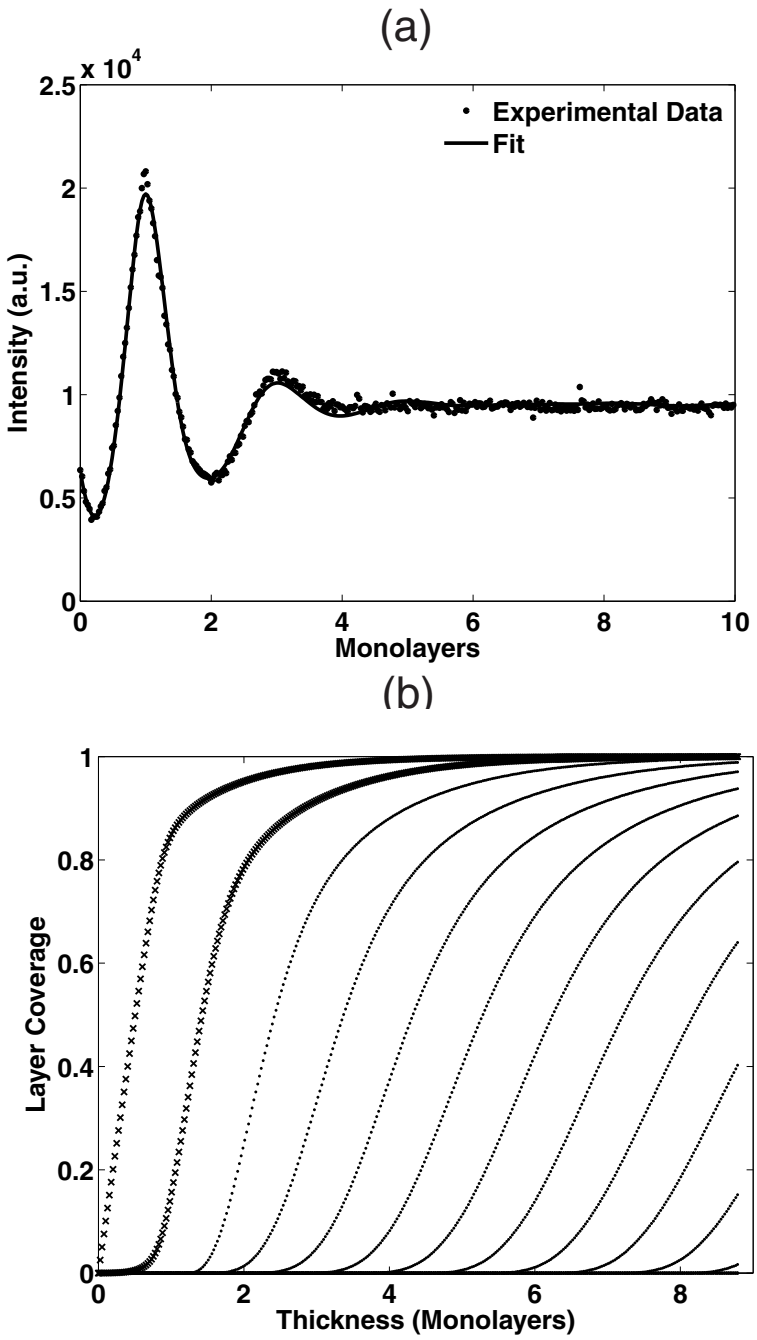

Figure 5.4: (a) Intensity oscillations and the fit to the cohen model (b) Layer coverages as observed for the growth at -16°C at 2.6 eV.

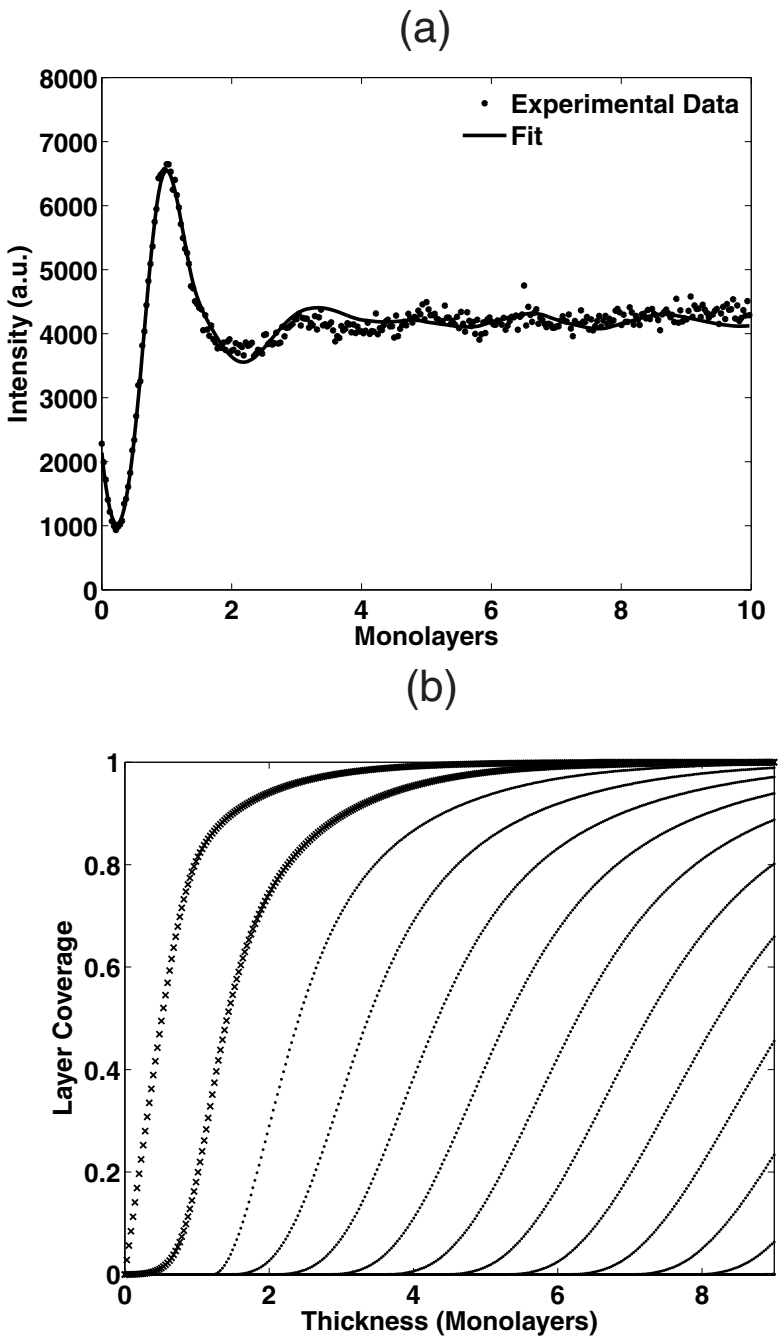

Figure 5.5: (a) Intensity oscillations and the fit to the cohen model (b) Layer coverages as observed for the growth at -66°C at 2.6 eV.

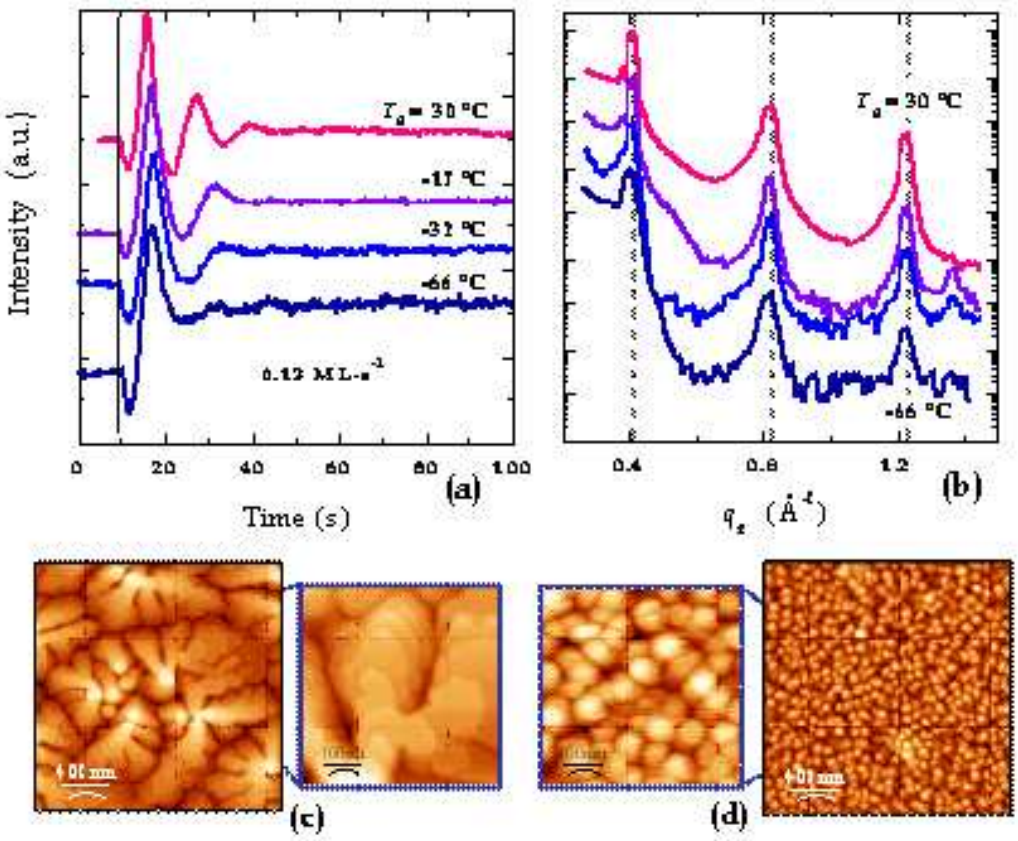

Figure 5.6: a) Intensity oscillations at different temperatures (b) X-ray reflectivity measurements with no evidence of the existence of new polymorphs (c) AFM of the film grown at room temperature (d) AFM of the film grown at a temperature of -66°C.

Chapter 6
Anomalous growth behavior of pentacene thin films

6.1 Overview

The deposition and growth of pentacene on thermal silicon dioxide has been examined using in-situ x-ray scattering and ex-situ using atomic force microscopy (AFM) and grazing incidence wide angle x-ray scattering. Pentacene films ($\sim$ 40 monolayers thick) were deposited on silicon dioxide at different growth rates varying from 0.008 ML-s^{-1} to ML-s^{-1}. As the growth rate was varied, different film morphologies varying from 2D layer by layer growth to 3D growth were observed. An "anomalous" behavior with regards to the film morphology was observed at high growth rates. Within the range of low to modest growth rates, initially 2D layer by layer growth was observed followed by 3D growth accompanied by the formation of islands and hence rough surface. In the anomalous regime (growth rate $>$ 0.4 ML-s^{-1}), persistent layer by layer (2D) growth was observed. It was also accompanied by a change in the crystalline structure of thin films. Ex-situ grazing incidence wide angle x-ray scattering (GIWAXS) was used to further analyze the films deposited at the anomalous growth rate. We observed the formation of another polymorph of pentacene. With the help of mass spectroscopy, dimers of pentacene were being formed, and concomitantly the onset of the formation of van-der-waals clusters coincided with the transition to the anomalous regime. The formation of clusters in the incident beam at high growth rates attributed to the change in the dynamics of thin film growth.

6.2 Introduction

The discovery that the electrical conductivity of polyacetylene, a conjugated polymer, could be tuned in such a way as to make it functional as an insulator, semiconductor or a metal is widely believed to have opened the floodgates on the use of organic materials in electronics [81]. Owing to their ability to form structures with transport characteristics superior to that of amorphous silicon (a-Si) [1, 52, 56], polyacene molecules such as pentacene, anthracene have drawn significant attention in the past two decades. This led to the incorporation of organic materials in electronic circuits with potential applications in thin film transistors, light emitting displays, printable electronic circuits and flexible devices such as RFID tags, sensor packs etc. with potential advantages being low cost, low processing temperature, a large choice of substrates and large area coverage. The preparation of a large variety of organic - inorganic hybrid materials with amazing properties has already been reported [82, 83].

Organic thin films have been traditionally deposited by thermal evaporation or by sublimation in vacuum. However, more recently techniques like pulsed laser deposition [62], organic vapor phase deposition [84] and supersonic molecular beam deposition have been gaining impetus. Simple processes like evaporation have been successful but provide limited ability to tune the film growth as deposition rate and substrate temperatures are the only process variables. The tendency of the thin films crystals to quickly undergo 3D growth and form pyramid like structures has already been reported [10, 85, 86]. Such rough surface morphologies, with tall pyramid like structures [10, 48, 87] are not applicable for device architecture as they provide a poor interface for dielectric or metal contact with the semiconductor.

Energetic processes such as ion beam deposition, sputtering, and plasma assisted deposition have become pervasive in the last few years due to the use of hyperthermal species (> 1eV) as they may favor development of new morphologies and structures.

Use of hyperthermal incident kinetic energies can lead to different surface collisional processes such as insertion and downward interlayer transport which attribute to the nucleation and growth of new crystal structures and promote 2D growth. Kang and Evans used surface diffraction techniques to understand the dynamics of atoms during deposition and post deposition transient mobility and their importance in downward interlayer transport and overcoming Ehrlich-Schwoebel barriers inhibiting transport from $(n+1)^{th}$ to n^{th} layer to promote layer by layer growth [88, 89]. Previous reports on molecular dynamics simulation have shown that hyperthermal impingement of clusters has a smoothing effect on the surface during the growth [43]. Meinander reported the effect of size and energy of the clusters on the cluster assembled thin films using molecular dynamics simulation. They found that at thermal energies small clusters align epitaxially while large clusters may form grains and islanded morphology [39]. Yamada and co-workers demonstrated the effect of incident kinetic energy of cluster beams for aluminum (Al) deposition on Si and CaF_2 and found through energetic deposition, lattice misfit can be accommodated at initial stages of film deposition and hence can give rise to smooth epitaxial films [90]. Computational methods have been used to understand the impact of the clusters with different energies on a surface. It has been found that super-hot (highly energetic) clusters hitting the surface at a supersonic speed tend to fragment and dissociate into small molecules [91]and can further lead to the smoothing of the film by a downhill movement at a step edge. Qi and Sinnott studied and simulated thin film growth through impact of hyperthermal acetylene clusters on diamond (111) and H-terminated diamond [42]. In the last few years anthracene and polyethylene films have been deposited by ionized cluster beam at thermal and hyperthermal energies and have been found that the films deposited at thermal energies were amorphous while the films deposited at high incident kinetic energies had crystalline structure [92]. Arias and co-workers studied the collisions between metal-oxide clusters

and surfaces through molecular dynamics and attributed the fast smoothing mechanism of films grown by pulsed laser deposition to the complete assimilation of the energetic clusters on the metal surface [93].

As discussed above, energetic clusters have a great impact on the morphology of thin films as they have a tendency to break on hitting the surface and either assimilate, melt or fragment or undergo downward funneling thus producing smooth and crystalline films. Organic molecules, as compared to inorganic molecules are more susceptible to breakdown and therein lay the challenge with regards to the techniques used for the energetic deposition of organic thin films. Supersonic molecular beam deposition has recently emerged as a powerful technique that provides an edge over other techniques like thermal deposition and pulsed laser deposition with regards to organic thin film deposition. These beams combine techniques to provide spatially well defined collision free flux of molecules with the seeding techniques which can be used to control the incident beam state like energy, momentum and flux. Hence by changing the seeding gas, incident kinetic energy and the beam flux can be tuned to produce van-der-waal clusters of molecules. Hagena et. al reported the formation of clusters in supersonic beams and the effect of pressure and temperature on cluster formation [18]. Iannotta and Milani concluded that the hyperthermal cluster beams produced by supersonic seeded methods have a great impact on the structure, morphology and functional properties of thin films [40].

It has been shown previously that pentacene, a molecule of great technological importance, can be deposited using seeding techniques in supersonic molecular beam deposition in hyperthermal energy range ($\sim$ 1 to 13 eV), without undergoing any chemical change [21]. This chapter deals with the effect of the deposition rate on the morphology of pentacene thin films deposited from a supersonic source seeded in a helium beam.

6.3 Experimental details

The equipment and the experimental procedure have been described in chapter 3. A brief description with specifics to this chapter is included in this section. Thin film deposition was carried in an ultra high vacuum (UHV) chamber, with the base pressure of $\sim$ 2 x 10^{-9} torr. Substrates were small samples ($\sim$ 12mm x 12 mm) cleaved from Si(100) 4" wafers. These 4" wafers were subjected to a RCA-1 clean, followed by HF dip and then RCA-2 clean immediately before the growth of thermal oxide, SiO_2($\sim$300 nm). The cleaved samples were then cleaned by 15 min sonication in $CHCl_3$ and 15 min sonication in deionized water. The samples are then dried by N_2 and cleaned with UV-Ozone for 10 min. Supersonic molecular beams of pentacene were them generated by passing a carrier gas (helium) over a heated evaporator (bubbler). Pentacene molecules seeded in helium pass through a nozzle (150μm orifice in a stainless steel plate), which then pass through a trumpet shaped skimmer (2.0 mm aperture, Beam Dynamics) into an antechamber and through a large aperture that produced a well defined circular beam spot on the substrate at normal incidence. The antechamber has a manually controlled shutter/flag which is used for the precise exposure of the substrate to the beam. The flow of the carrier gas can be modulated using the mass flow controller (MKS type). The growth rate can be controlled using by varying the temperature of the bubbler/evaporator, as the temperature of the bubbler control the amount of pentacene evaporating and seeding in to the helium gas passing though it. Beam energy of 2.7eV was by time of flight experiments by seeding pentacene in 10 sccm of Helium. The pentacene flux can be modulated using by varying the temperature of the evaporator (Tb) between 220°C to 320°C, thus giving a deposition rate varying between 0.008ML-s^{-1} to 2ML-s^{-1}. The nozzle pressure remained stable at 58 torr until the temperature rose above 280°C, after which it increased significantly. The thickness of pentacene films grown is $\sim$40 monolayers.

The chamber is mounted on a diffractometer table for an in-situ analysis using x-ray diffraction, which completely eliminates the differences caused in the film morphology by post growth thin film restructuring. The incoming flight path allow the x-ray to pass through the horizontally mounted Be window. The incident x-rays are scattered from the depositing pentacene layer. These scattered x-rays then pass through the vertically mounted Be window and through the ion chamber pass through the Bede scintillator counter to measure the intensity of the scattered x-rays. This is obtained as a graph of intensity versus time, where the oscillations give an idea of the morphology of the films. The intensity oscillations thus obtained are fitted to a modified cohen model to obtain the fitting parameters which, along with ex-situ atomic force microscopy (AFM) indicate if the film is amorphous or has tall islands with deep trenches or is smooth.

6.4 Results and Discussion

Pentacene films grown by supersonic molecular beam deposition were analyzed in-situ using anti-bragg scattering and ex-situ using atomic force microscopy. X-ray scattering measurements such as anti-bragg scattering, x-ray reflectivity measurements are a powerful tool used to characterize films and enable real time monitoring of film thickness and surface roughness during growth. Anti Bragg scattering has been widely used to characterize growing films in order to maximize the sensitivity to the surface roughness and the growth mode (layer by layer or 3D) [21, 94].

6.4.1 Qualitative analysis

Pentacene films were grown on SiO_2 with incident kinetic energy being 2.7eV or 4.5eV, substrate temperature set to $30°C$ (= room temperature) and the incident flux being modulated by controlling temperature of the evaporator containing pentacene, which

modulates the partial pressure of pentacene, thus producing growth rates varying from 0.008 ML-s^{-1} to 2 ML-s^{-1}. The incident x-rays passing through a Be window had an energy of 9.8keV. Time resolved intensity measurements and θ-2θ scans were performed in the anti-bragg configuration. Figure 6.1(a), 6.2(a), 6.3(a) shows the X-ray intensities obtained at the anti-bragg condition for three sets of growth rate - 0.008 ML-s^{-1}, 0.8 ML-s^{-1} and 2ML-s^{-1} respectively. The oscillations damp out gradually indicating that the films roughen as they become thicker. The local maxima obtained in the anti-bragg oscillations correspond to an integral number of layers, which implies that the first oscillation corresponds to 2 monolayers of pentacene.

Figure 6.1(a) gives the x-ray intensity oscillation and the fit to the cohen model at the lowest deposition rate of 0.008 ML-s^{-1}. There is a perfect cusp at the peak of the first oscillation, which corresponds to the completion of the first layer before the second layer starts to nucleate. Figure 6.1(b) shows the evolution of the layer coverage as the film grows as a function of the total coverage in monolayers. It is evident in Figure 6.1(b) that the second layer nucleates after the completion of the first layer. This has been observed previously for growths with thermal deposition and supersonic molecular beam deposition [32]. As the film grows beyond the first monolayer, significant damping of the oscillations is observed. This corresponds to the roughening of the films and substantiates that the film is becoming three-dimensional.

The growth rate is gradually increased to 0.8 ML-s^{-1} and then to 2 ML-s^{-1}. As seen in Figure 6.2(a) and 6.3(a) the intensity oscillations at higher growth rates are more sustained (4 and 7 complete oscillations observed for growth rate of 0.8 and 2 ML-s^{-1} respectively) and the oscillation damp out gradually indicating

1. 2D growth is more prominent at higher growth rates
2. Roughening process and the transition to 3D growth is slow and happens gradually.

The evolution of the layer coverages at a growth rate of 0.8 and 2 ML-s^{-1} as shown in Figure 6.2(b) and 6.3(b) also indicate the same. Ex-situ atomic force microscopy, in tapping mode, was used to obtain images to understand the evolved morphology at the three growth rates. Figures 6.4 represent the AFM images obtained at 0.008 ML-s^{-1}, 0.8 ML-s^{-1} and 2 ML-s^{-1}. The AFM of the film deposited at lowest growth rate exhibit tall pyramid like structures (as shown earlier for thermal [10] and supersonic deposition [40], while the films at higher growth rate are smoother. Underneath the AFM images, are the corresponding histograms for each growth rate representing the exposed coverages for each monolayer of film deposited.

The histogram represents the exposed coverage for each layer of pentacene being deposited on SiO_2. The fit of the intensity data to the modified Cohen model generates a file which contains information about the coverages on each layer. The exposed coverage for each layer can be calculated from the file. For the film deposited at 0.008 ML-s^{-1}, as shown in Figure 6.4, the histogram is broad and nearly Gaussian with approximately 60 layers exposed. The skewness of the histogram with a tail extending towards the film/vacuum interface represents that the formation of a wedding cake like morphology, indicative of a significant Ehrlich-Schwoebel barrier to the downhill transport of the molecules, thus preventing a layer by layer growth [95]. At higher growth rates, the number of exposed layers has decreased. The maximum, in the height distribution, lies above the mean which suggests that the height distribution is slightly skewed and there exist very few low pits which are still unfilled. It is quiet evident from anti-bragg scattering, AFM and the height distribution that increasing growth rate (deposition rate) promotes 2D layer by layer growth. Fit of the intensity oscillations for the lowest deposition rate to the modified version of the Cohen model (Figure 6.1(a))gives parameters where A1>A2>An where A1 is very close to 1. This clearly suggests that first layer is formed completely indicating a layer by layer growth while after the growth of the

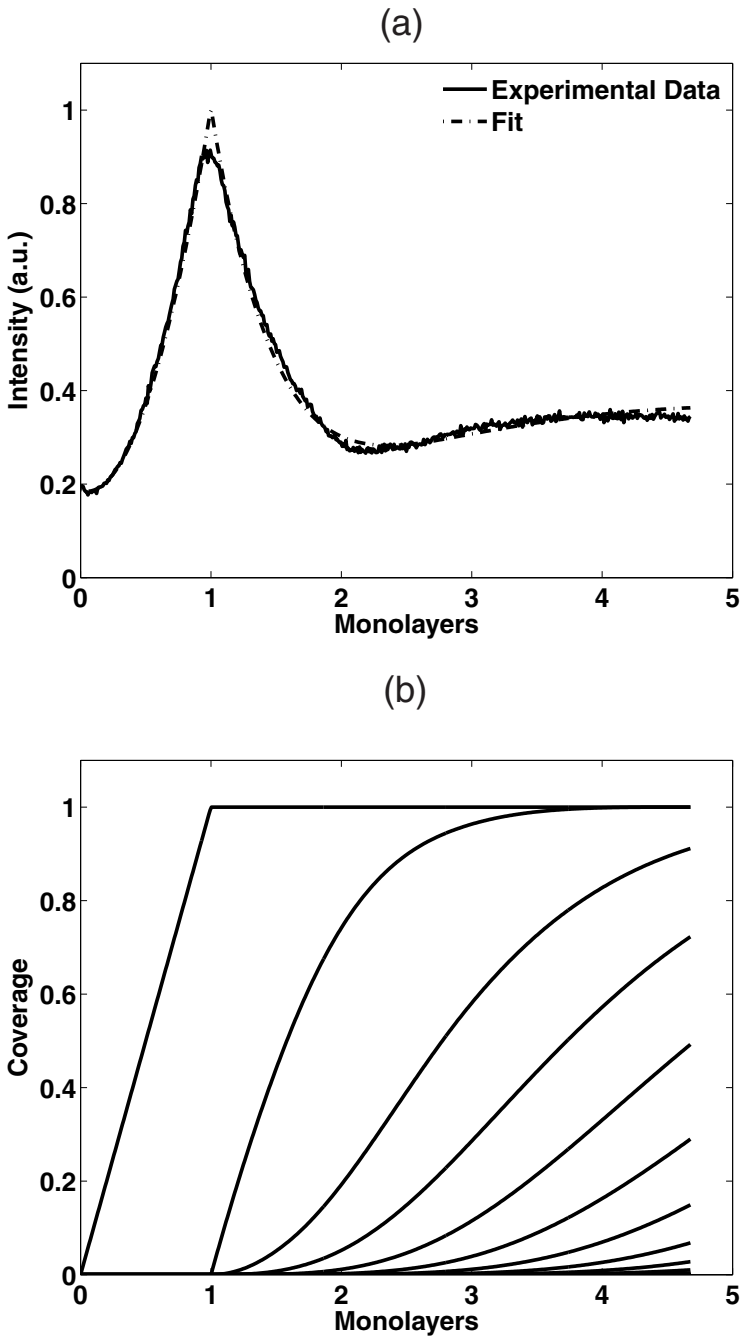

Figure 6.1: (a) Intensity oscillations and fit to the Cohen model (b) Layer coverage at a growth rate of 0.008 ML-s^{-1} at 30°C at 2.6 eV.

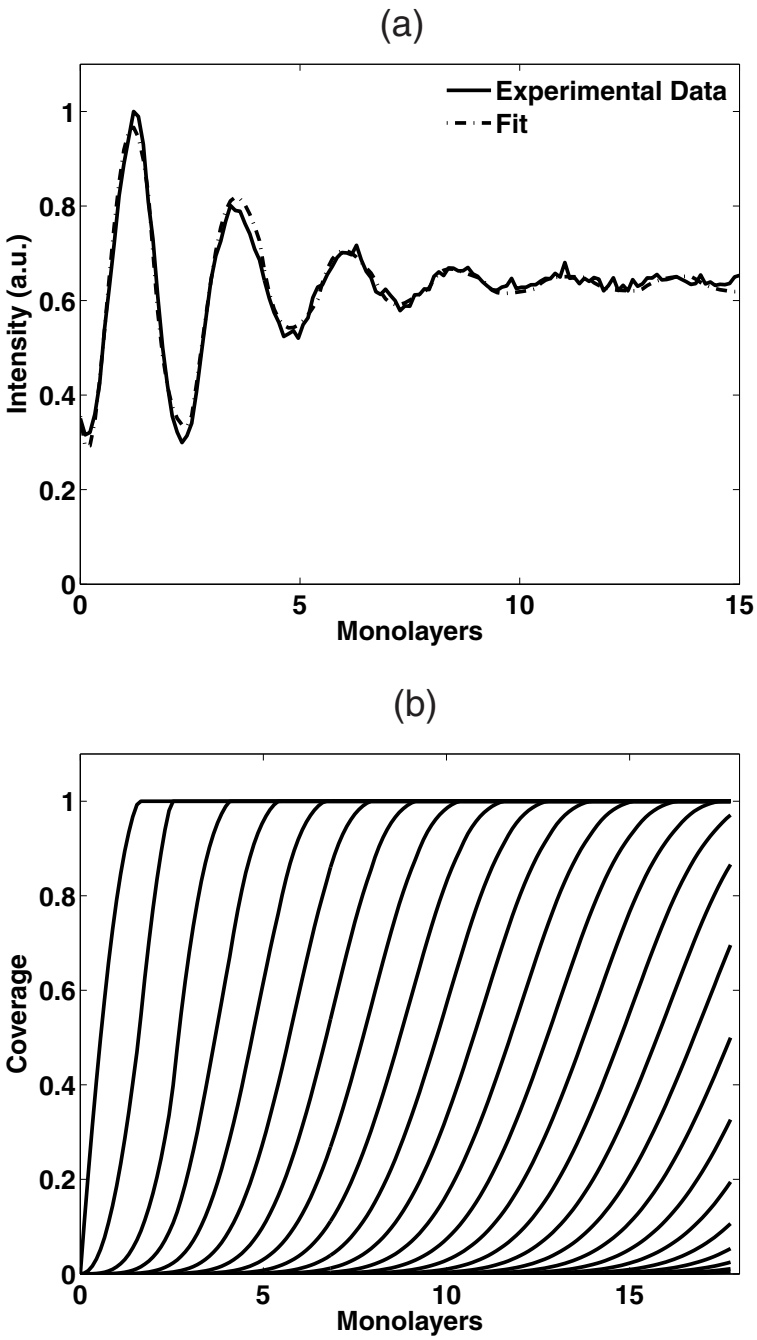

Figure 6.2: (a) Intensity oscillations and fit to the Cohen model (b) Layer coverage at a growth rate of 0.80 ML-s^{-1} at 30°C at 2.6 eV.

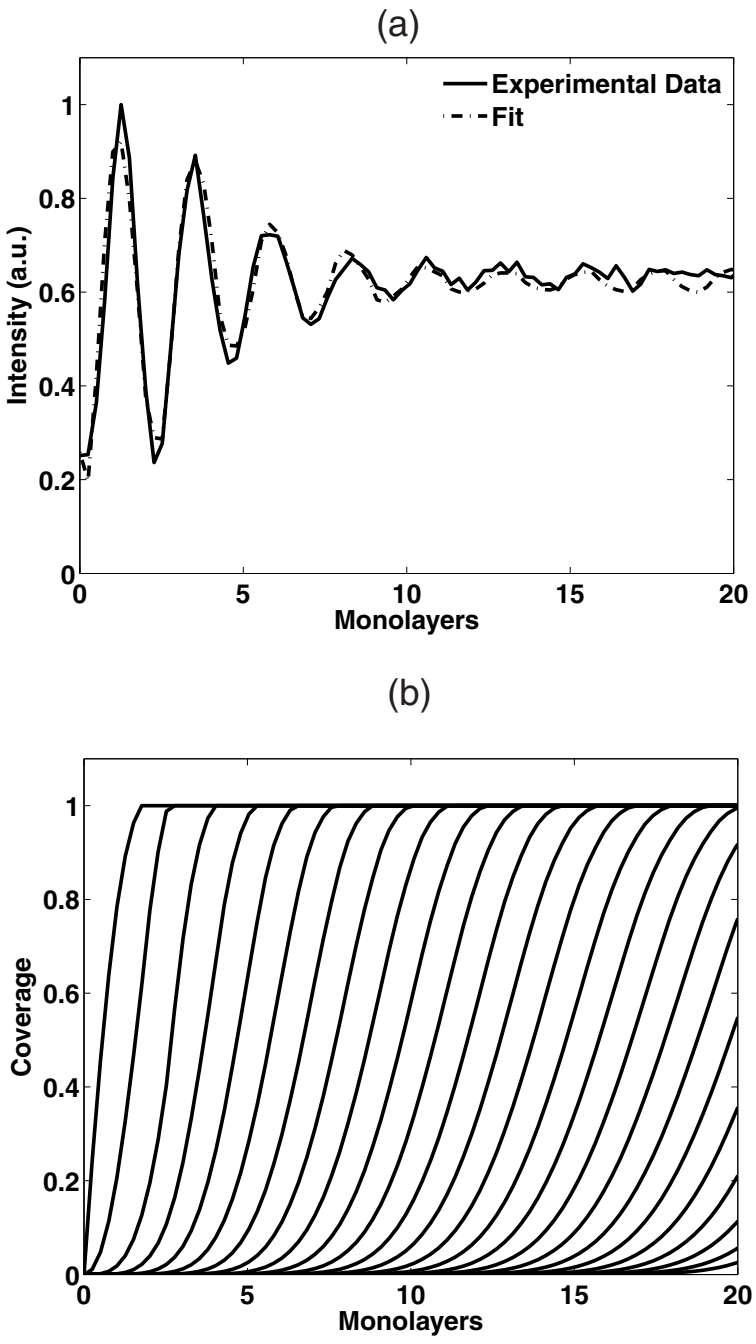

Figure 6.3: (a) Intensity oscillations and fit to the Cohen model (b) Layer coverage at a growth rate of 2 ML-s^{-1} at 30°C at 4.5 eV.

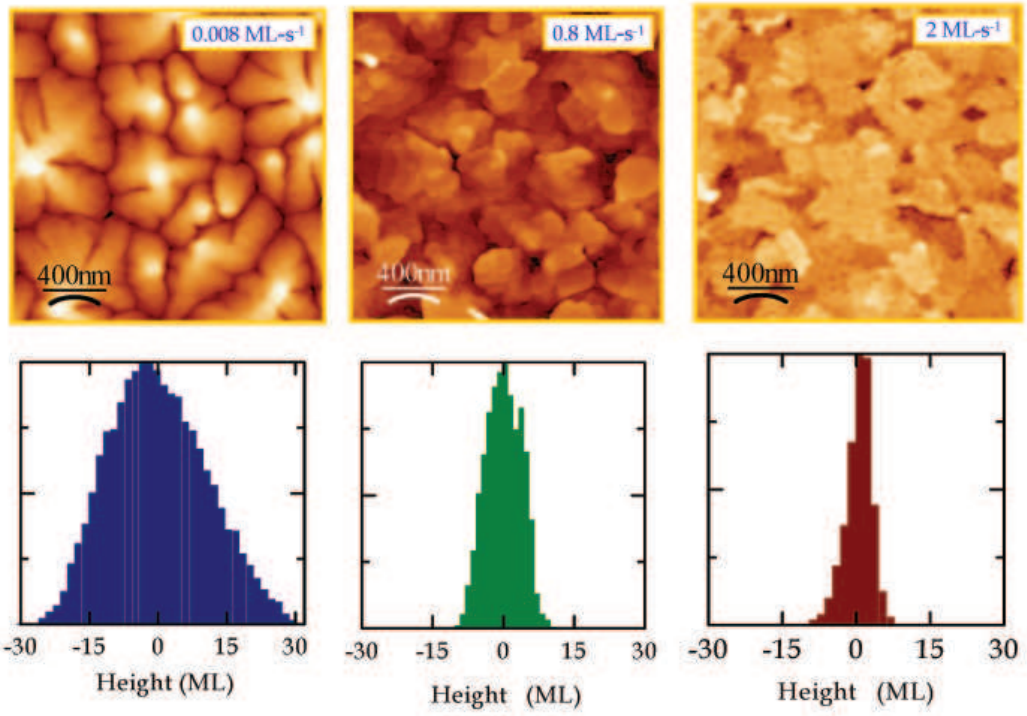

Figure 6.4: AFM images and corresponding height distribution for the growth rates of 0.008, 0.8 and 2 ML-s^{-1}.

first monolayer island begin to form on top of the incomplete monolayers as indicated by a value of A2 = 0.440.007. At high growth rates, we observe that A1<A2 which suggest that even though the second monolayer starts to develop before the first one is complete there are few trenches A2>An which indicates that a very small number of islands nucleate on top of incomplete monolayers.

Reflectivity measurements, as shown in Figure 6.5, on pentacene films reveal significant structural changes at low and high deposition rates. Existence of sharp 00L peaks at both 0.008 ML-s^{-1} and 2ML-s^{-1} show that the films are highly textured. From Bragg's law, d-spacing (inter-planar spacing) can be evaluated for both the thin film and the bulk phase (if observed) at all the three growth rates. At low growth rates the crystallites were found to consist mainly of thin film phase (d_{001} = 15.4 Å), with a d-

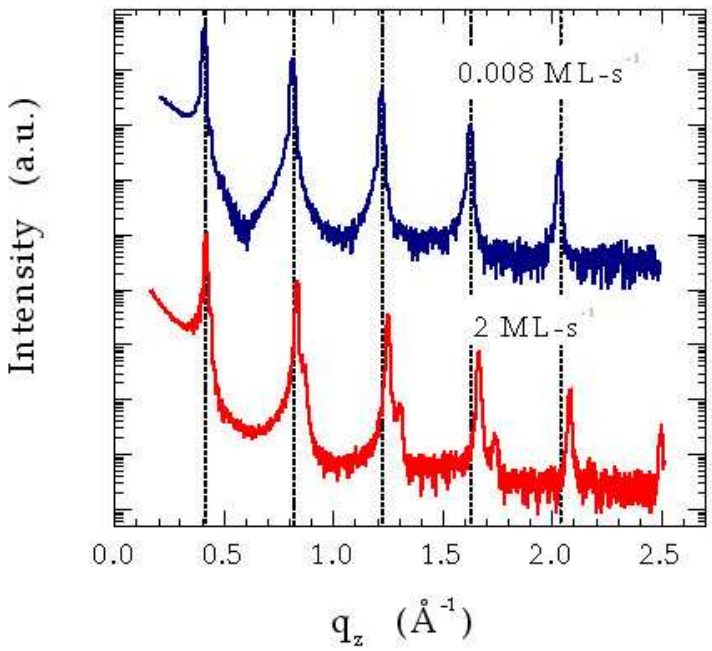

Figure 6.5: Reflectivity measurements showing the existence of a new polymorph for the film grown at 2 ML-s^{-1}.

spacing of 15.37±0.04 Å. At high growth rates, a bimodal structure is observed with two distinct 00L peaks and two different inter planar spacing. The first 00L peak is observed at a d-spacing of 15.15±0.03 Å close to d_{001} of 15.1 Å (a pentacene polymorph) which was observed by Wu and Spence [37] during electron diffraction of pentacene grown on NaCl. Another 00L peak is observed at a d-spacing of 14.77±0.02 Å, which is larger than the inter planar spacing obtained for bulk phase is equal to 14.5 Å. Ex-situ grazing incidence wide angle x-ray scattering (GIWAXS) also reveal the existence of a polymorph of pentacene by determination of lattice parameters at high deposition rates. The bright spots in Figure 6.7 correspond to the peaks on a crystal truncation rod. For a film grown at the lowest growth rate, we observe a 3-2-3 pattern of the peak, which corresponds to the triclinic phase of pentacene molecules. However at higher growth

rates, through calculation using MathCAD, we find that the lattice parameters are close to monoclinic structure as shown in Figure 6.7.

6.4.2 Onset of clustering

As observed above in Figures 6.1 to 6.5, we observe a drastic change in the growth dynamics at high growth rates. Figure 6.6(a) gives a graphical presentation of the number of maxima in the x-ray intensity oscillations at the anti-bragg condition changing with the growth rate. As the growth rate is increased, the number of peaks is almost the same for a deposition rate between 0.008 ML-s^{-1} and 0.4 ML-s^{-1}, however the number of oscillation sharply increase with the growth rate increasing beyond 0.4 ML-s^{-1}, indicating a distinctly different growth behavior. Figure 6.6(b) represents the plot of out-of-plane interplanar spacing versus the deposition rate. As low growth rates (0.008 ML-s^{-1}<GR<0.4 ML-s^{-1}), we observe the existence of thin film phase for almost all the films. This is similar to what has been observed earlier for thermal and hyperthermal depositions. The film at the lowest growth rate shows the presence of a bimodal phase where both thin film and bulk phases co-exist. This has been reported earlier by Malliaras and co-workers where they determined that the bulk phase nucleates at the start of the first monolayer and as the film thickens, it shadows the thin film phase [33, 96].

6.4.3 Formation of polymorphs of pentacene

The electronic properties of an OTFT depend on the way pentacene molecules stack on the substrate. Pentacene is known to crystallize with a herringbone structure and has shown the existence of two phases ”thin film”, at an inter-planar of 15.4 Å and ”bulk phase”, at an inter-planar spacing of 14.5 Å. The existence of different polymorphs of

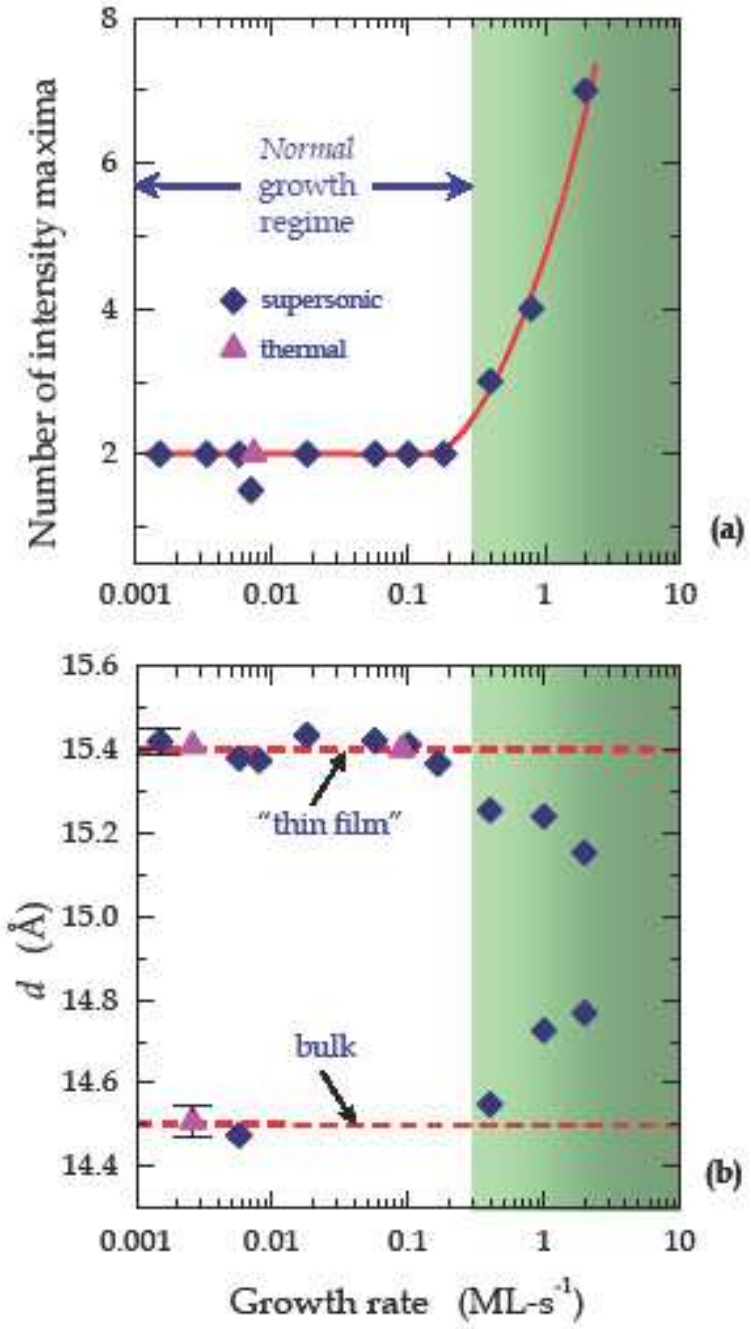

Figure 6.6: (a) Steep increase in the number of intensity maxima beyond 0.4 ML-s^{-1}.(b) Change in the inter-layer spacing with the increase in the growth rate (*Private Communications with Dr. Aram Amassian).*

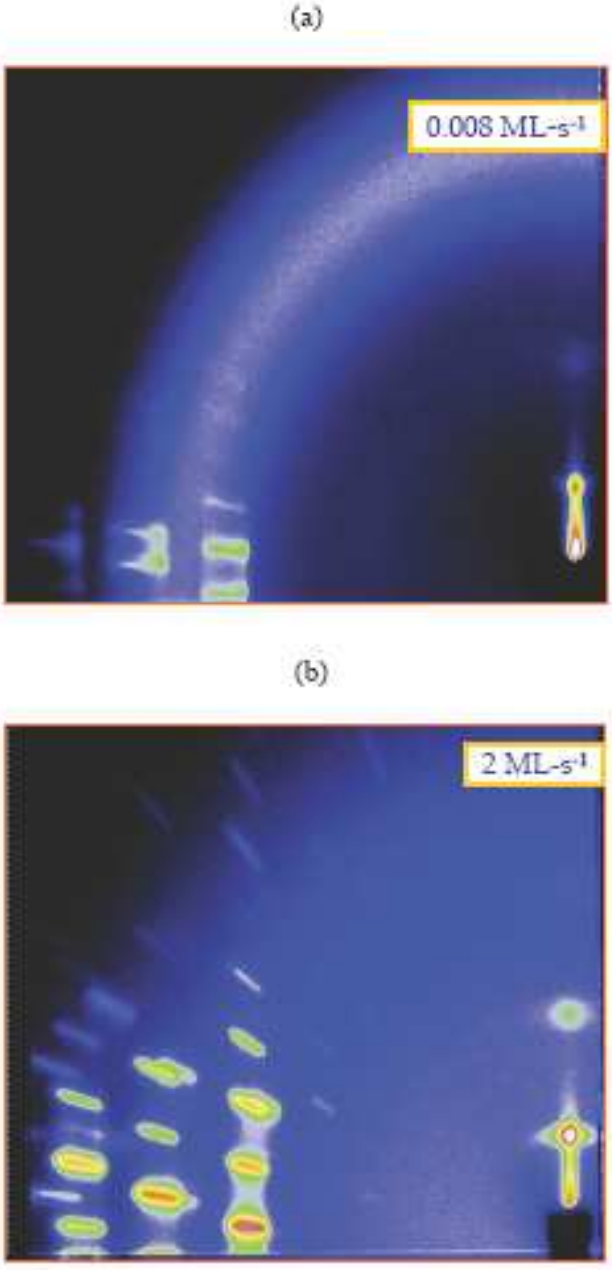

Figure 6.7: Existence of polymorphs as shown by GIWAXS measurements for growth at 2 ML-s^{-1}.

pentacene, with a d-spacing of 14.1 Å (Holms et.al (1999)), 14.5 Å [24] has already been reported previously. Mattheus and co-workers reported, through electron diffraction, the formation of four polymorphs of pentacene with a d-spacing of 14.1 Å, 14.4°A, 15.0 Å and 15.4 Å [97]. All of these polymorphs can be formed in the thin film phase depending on the growth conditions. Dimitrakopoulos and co-workers reported the formation of a single-crystal phase and a metastable thin film phase in pentacene films deposited by molecular beam deposition and characterized by x-ray diffraction and scanning electron microcopy [33]. Bouchoms and co-workers identified two crystallographic phases of vacuum evaporated pentacene on SiO_2 through AFM and θ-2θ x-ray measurements. They determined the thin film phase consisting of strongly faceted grains with a inter-planar spacing of 15.5 Å, and the triclinic bulk phase consisting of lamellar structures with an inter-planar spacing of 14.5 Å [34]. Low substrate temperatures and films grown on different substrates other than SiO_2 also show thin films with d-spacing of 15.0Å and 15.4 Å.

The films grown by supersonic molecular beam deposition at a room temperature at varying deposition rates show three different polymorphs, with a d-spacing of 14.77 Å, 15.15Å and 15.25 Å. It has been reported for heteroepitaxial GaAs-Al interface that the broadening of the diffraction peaks point to the development of strain in the films. However since no such broadening is observed for pentacene grown on SiO_2 by supersonic beams, there is no strain development in the films [98].

6.4.4 Energetic clusters of pentacene

As observed above, a change in the crystal structure and a transition to an anomalous regime is seen at a growth rate > 0.4 ML-s^{-1}. This cannot be solely attributed to an increase in the growth rate, since we observe a drastic increase in the nozzle pressure (stagnation partial pressure of pentacene behind the nozzle) along with structural changes,

Table 6.1: Effect of growth rate on the partial pressure of pentacene.

Growth Rate (ML-s^{-1})	Mole fraction of pentacene	Partial pressure of pentacene (Torr)
0.13	0.042	< 1
0.40	0.080	26
0.80	0.300	110
2.00	0.260	180

which is shown in Table 6.1. In supersonic expansions van-der-waal clusters (dimers and trimers) have a high formation probability at high stagnation pressures. It has been reported previously by Beijerinck and Hagena [16, 99] that van-der-waal clusters of pentacene are formed in supersonic expansion and this can be related to the value of a dimensionless group called as C^*, which is defined as:

$$C^* = \frac{P_n d^{0.88} T_n^{-23}}{\sigma^{0.88 \frac{\epsilon}{\sigma^3}} (\frac{\epsilon}{k})^{-2.3}} \tag{6.1}$$

P_n and T_n are the stagnation nozzle pressure and nozzle temperature respectively, d is the nozzle diameter (= 125μm), k_B is the Boltzmann's constant, e and s are the Lennard-Jones (L-J) potential parameters for the vapor phase. They reported that the value of C^* should be > 15 for the formation of van-der-waal clusters of supersonic beams of monoatomic gas. The value of Lennard-Jones parameters, ϵ and σ, are obtained from the ab-initio quantum chemical calculations (GAUSSIAN98 [100]) by assuming a variety of geometrical scenarios for dimer formation. The value obtained for ϵ and σ are 0.55 eV and 3.3 Å respectively To calculate C^*, the presence of the carrier gas is ignored and Pn is replaced with partial pressure of pentacene (P(C22H14)). This assumption is reasonable because of the huge mass difference between carrier gas and pentacene. The C^* calculated for growth rate > 0.4 ML-s^{-1} is ~20 (Figure 6.8) which confirms the

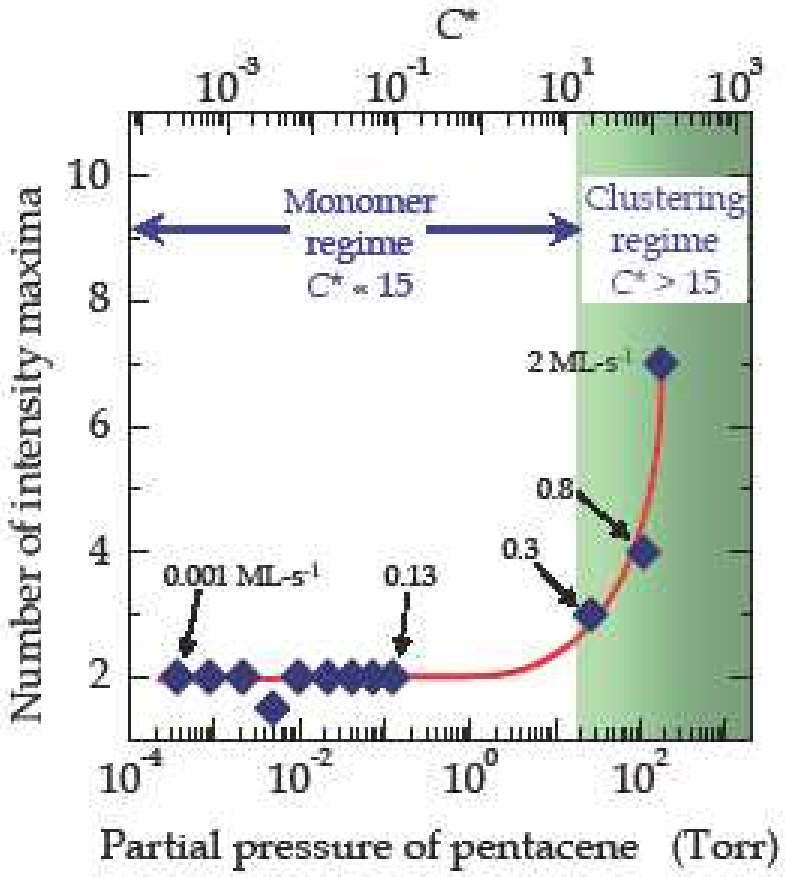

Figure 6.8: Effect of the partial pressure of pentacene on the number of intensity maxima (*Private Communications with Dr. Aram Amassian).*

formation of pentacene clusters in the molecular beam. The value of C^* for GR=0.13 ML-s^{-1} is << 1, hence no clusters are formed. The value of C^*>15 confirms the formation of clusters. This was further complemented by some preliminary experiments with the quadrupole mass spectrometer. The mass spectrometer (quadrupole Extrel type) was mounted on the chamber to be in direct line of sight of the molecular beam at ~40 cm away from the sample. The problem with the mass spectrometer lies in the fact that the clusters can undergo fragmentation due to the electron impact and formation of ions as reported by Buck and Meyer for Argon clusters (Buck et. al (1984)). Molecular

beams were analyzed at two different growth rates, one in the normal regime i.e. GR < 0.13ML-s^{-1} and the other at a GR > 0.4 ML-s^{-1}. Figure 6.9(a) and (b) represents the mass spectra regions for monomers (m/e = 278) and dimers (m/e = 556) of pentacene in the normal and the anomalous (clustering) growth regime respectively. From the mass-spec experiments, the peak occurs with molecular mass varying between 552 to 561 a.m.u. However, whether the cluster are bonded by van-der-waal forces or by chemical interactions is a topic of further research.

To represent if the onset of the formation of dimers coincides with the growth rate at which C^* is observed to be > 15, a graph between the intensity of dimer peak versus the growth rate is plotted (Figure 6.9(c)). Figure 6.8 correlates the number of peaks in the anti-bragg oscillation with the partial pressure of pentacene as observed over the entire range of growth rates. From figures 6.8, 6.9(c), 6.6(a) and 6.6(b), it can be concluded that there exists a correlation between the onset of formation of clusters and the structural changes (extended 2D growth, more number of intensity oscillations) observed in the supersonic deposition of pentacene on SiO_2. The formation of clusters is an important feature leading to a layer by layer growth thus an efficient inter-layer transport. Usually the factors promoting a layer by layer growth are high substrate temperatures and low growth rates. Figure 6.1(a) indicates the presence of a sizable Ehrlich-Schwoebel barrier exists which is evident from the fast transition to the 3D growth. The anomalous growth regime where film smoothening was observed can be attributed either to high growth rates at which the film was grown or to the formation of clusters in molecular beam or both. Usually, if the higher growth rate at a fixed substrate temperature gives an efficient inter-layer transport, then decreasing substrate temperature at a fixed growth rate should show a similar behavior. As explained in section 5.2.3, pentacene was grown on SiO_2 at different substrate temperature varying from 30 to -66°C. The oscillations were observed at a temperature as low as -66°C,

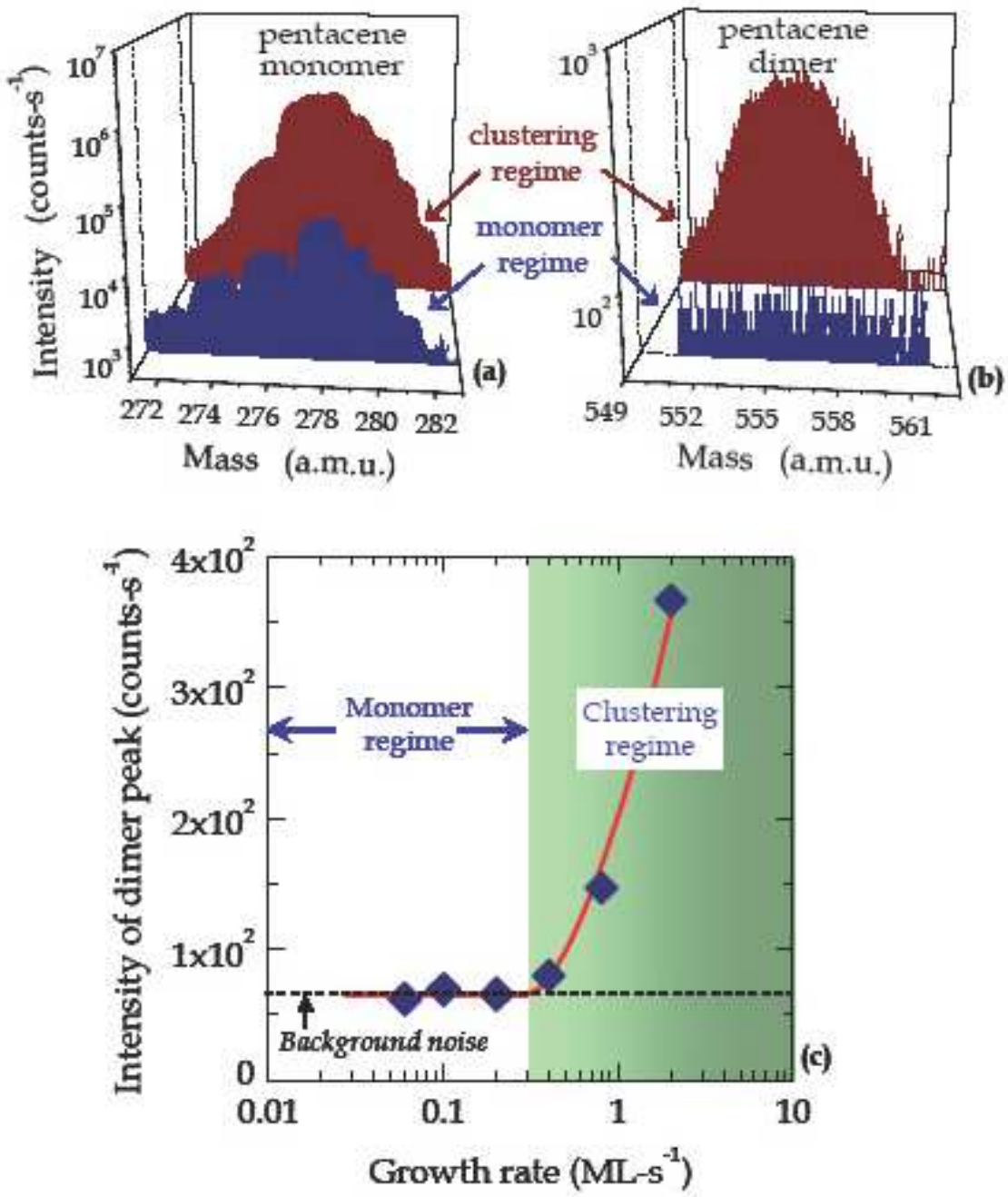

Figure 6.9: Onset of clustering versus growth rate, formation of pentacene dimers (*Private Communications with Dr. Aram Amassian).*

but the oscillations damp out faster as the temperature is reduced. The AF micrographs show that the films grown at -66°C exhibit a cauliflower like morphology as opposed to the terraced morphology exhibited by the films grown at 30°C. There was no evidence of any structural changes observed by in-situ x-ray analysis. It is quite evident from these facts that the effect of decreasing substrate temperature is opposed to the effect of increasing growth rate and thus a higher growth rate is not the only reason for facilitating 2D growth.

The fact that onset of clustering coincides with the anomalies observed in the growth dynamics further assure that clustering is a major phenomena affecting the growth dynamics of thin films at high growth rates. Clustering can give rise to a 2D smooth surface because upon collision, the dimers of pentacene lead to an efficient momentum transfer due to equal mass of the molecules. This can give rise to two possible consequences. If the clusters survive the impact, they lead to the formation of a high density of small islands with irregular step edge geometry which enhances inter-layer transport thus promoting a layer by layer growth. In the second case, the hyperthermal clusters can break islands and detach molecules from the islands and from the step edges. Such collisional processes at hyperthermal energies can produce surface modifications which can change inter-layer transport thus affecting the film morphology and the structure of the films and promoting smoothening of the films as reported by Toyoda et.al [44] and Yamada et.al [90].

6.5 Conclusion

Pentacene has been deposited on SiO_2 substrates at different growth conditions such as growth rate, kinetic energy of the incident molecules and substrate temperature using a supersonic molecular beam. Using the supersonic molecular beams and varying the growth rate from 0.008 ML-s^{-1} to 2.0 ML-s^{-1} can produce spectacular impact on the

growth dynamics and the morphology of organic thin films. The results shown in this chapter indicate that films grown at high growth rate exhibit smoother morphology and prohibit the development of rough structures and this is attributed to the formation of clusters incident at high kinetic energies.

BIBLIOGRAPHY

[1] C. D. Dimitrakopoulos and P. R. L. Malenfant. *Advanced Materials*, 14:99, 2002.

[2] C. Reese, M. Roberts, M.-M. Ling, and Z. Bao. *Materials Today*, 7:9, 2004.

[3] S. M. Sze. *Physics of semiconductor devices*. John Wiley and Sons: New York, 2 edition, 1981.

[4] M. J. Madou. *Fundamentals of Microfabrication:Tthe science of miniaturization*. CRC Press: New York, 2002.

[5] J. B. Anderson. *Molecular Beams and Low density gas dynamics*. Marcel Dekker: New York, 1974.

[6] G. Scoles. *Atomic and Molecular Beam Methods*, volume 1. New York: Oxford University Press, 1988.

[7] A. Gibaud, D. Mc Morrow, and P. P. Swaddling. *Journal of Physics: Condensed Matter*, 7:2645, 1995.

[8] A.C Mayer. *Growth and structure dynamics of pentacene : thin films with applications to OTFTS and OPVS*. PhD thesis, Cornell University, 2006.

[9] P. I. Cohen, G. S. Petrich, P. R. Pukite, and G. J. Whaley. *Surface Science*, 216:222, 1989.

[10] R. Ruiz, D. Choudhary, B. Nickel, T. Toccoli, K. C. Chang, A. C. Mayer, P. Clancy, J. M. Blakely, R. L. Headrick, S. Iannotta, and G. G. Malliaras. *Chemistry of Materials*, 16:4497, 2004.

[11] T.W. Schroeder. *Thin Film Deposition Employing Supersonic Molecular Beams : Nucleation and Growth of Silicon, Silicon Germanium and Pentacene*. PhD thesis, Cornell University, 2004.

[12] G. E. Moore. *Electronics*, 38, 1965.

[13] D. Eres and J. Z. Lowndes, D. H.and Tischler. *Applied Physics Letters*, 55:1008, 1989.

[14] S. Iannotta and T. Toccoli. *Journal of Polymer Science B*, 41:2501, 2003.

[15] M. F. Danisman, L. Casalis, and G. Scoles. *Physical Review Letters B*, 72:085404, 2005.

[16] O. F. Hagena. *Surface Science*, 106:101, 1981.

[17] T. A. Milne, J. E. Beachey, and F. T. Greene. *Journal of Chemical Physics*, 57:2221, 1972.

[18] O. F. Hagena and W. Obert. *Journal of Chemical Physics*, 56:1793, 1972.

[19] Buck U. and H. J. Meyer. *Surface Science*, 156:275, 1985.

[20] Buck U. and H. J. Meyer. *Chemical Physics*, 84:4854, 1986.

[21] A. Woll, R. L. Headrick, S. Kycia, and J. D. Brock. *Physical Review Letters*, 83:4349, 1999.

[22] D. J. Gundlach, Y. Y. Lin, T. N. Jackson, S. F. Nelson, and D. G. Schlom. *IEEE Electron device letters*, 18:87, 1997.

[23] S. E. Fritz, S. M. Martin, C. D. Frisble, M. D. Ward, and M. F. Toney. *Journal of American Chemical Society*, 126:4084, 2004.

[24] R. B. Campbell, J. M. Robertson, and J. Trotter. *Acta Crystallographica*, 15:289, 1962.

[25] D. Kafer, L. Ruppel, and G. Witte. *Physical Review Letters B*, 75:085309, 2007.

[26] A. S. Killampalli and J. R. Engstrom. *Applied Physics Letters*, 88:143125, 2006.

[27] R. Ruiz, B. Nickel, N. Koch, L. C. Feldman, R. F. Haglund, A. Kahn, F. Family, and G. Scoles. *Physical Review Letters*, 91:136102, 2003.

[28] M. Tejima, K. Kita, K. Kyuno, and A. Toriumi. *Applied Physics Letters*, 85:3746, 2004.

[29] D. Knipp, R. A. Street, B. Krusor, R. Apte, and J. Ho. *Journal of non-crystalline solids*, 1042:299, 2002.

[30] D. Guo, S. Ikeda, and K. Saiki. *Thin Solid Films*, 515:814, 2006.

[31] F. De. Angelis, T. Toccoli, A. Pallaoro, N. Coppede, L. Mariucci, G. Fortunato, and S. Iannotta. *Synthetic Metals*, 146:291, 2004.

[32] A. S. Killampalli, T. W. Schroeder, and J. R. Engstrom. *Applied Physics Letters*, 87:439, 2005.

[33] C. D. Dimitrakopoulos, A. R. Brown, and A. Pomp. *Journal of Applied Physics*, 80:2051, 1996.

[34] I. P. M. Bouchoms, W. A. Schoonveld, J. Vrijmoeth, and T. M. Klapwijk. *Synthetic Metals*, 104:175, 1999.

[35] T. Kakudate, N. Yoshimoto, and Y. Saito. *Applied Physics Letters*, 90:081903, 2007.

[36] A. B. Mattheus, C. C. andDros, J. Baas, A. Meetsma, J. L. de Boer, and T. T. M. Palstra. *Acta Crystallographica*, C57:939, 2001.

[37] J. S. Wu and J. C. H. Spence. *Journal of Applied Crystallography*, 37:78, 2003.

[38] P. S. Abthagir, Y. G. Ha, E. A. You, S. H. Jeong, H. S. Seo, and J. H. Choi. *Journal of Physical Chemistry B*, 109:23918, 2005.

[39] K. Meinander, T. T. Jarvi, and K. Nordlund. *Applied Physics Letters*, 89:253109, 2006.

[40] S. Iannotta and P. Milani. *AIP conference proceedings*, 576:979, 2001.

[41] S.J. Cho, M. K. Choi, S. O. Kim, J. K. Song, H. M. Yoon, S. H. Jin, T. W. Kwon, H. S. Woo, and D. K. Park. *Journal of Crystal Growth*, 288:140, 2006.

[42] L. Qi and S. B. Sinnott. *Journal of Vacuum Science and Technology A*, 16:1286, 1998.

[43] Z. Insepov, I. Yamada, and M. Sosnowski. *Journal of Vacuum Science and Technology A*, 16:981, 1997.

[44] N. Toyoda, N. Hagiwara, J. Matsuo, and I. Yamada. *Nuclear Instruments and methods in Physics Research B*, 980:161, 2000.

[45] J.R. Engstrom, D.A. Hansen, M.J. Furjanic, and L.Q. Xia. *Journal of Chemical Physics*, 99:4051, 1993.

[46] S. E. Roadman, N. Maity, J. N. Carter, and J. R. Engstrom. *Journal of Vacuum Science and Technology A*, 16:3423, 1998.

[47] L. Casalis, M. F. Danisman, B. Nickel, G. Bracco, T. Toccoli, S. Iannotta, and G. Scoles. *Physical Review Letters*, 90:206101, 2003.

[48] F. J. Meyer zu Heringdorf, M. C. Reuter, and R. M. Tromp. *Nature*, 412:517, 2001.

[49] M. Shtein, J. Mapel, J. B. Benziger, and S. R. Forrest. *Applied Physics Letters*, 81:268, 2002.

[50] S. Pratontep, M. Brinkmann, F. Nüesch, and L. Zuppiroli. *Synthetic Metals*, 146:387, 2004.

[51] H. Yanagisawa, T. Tamaki, M. Nakamura, and K. Kudo. *Thin Solid Films*, 464:398, 2004.

[52] Y. Y. Lin, D. J. Gundlach, S. F. Nelson, and T. N. Jackson. *IEEE Electron Device Letters*, 18:606, 1997.

[53] D. Knipp, R. A. Street, A. Volkel, and J. Ho. *Journal of Applied Physics*, 93:347, 2003.

[54] S. R. Forrest. *Chemical Review Letters*, 97:1793, 1997.

[55] A. Brown, C. Jarrett, D. de Leeuw, and M. Matters. *Synthetic Metals*, 88:37, 1997.

[56] G. Horowitz. *Advanced Materials*, 10:365, 1998.

[57] J. Venables. *Introduction to Surface and Thin Film Processes*. Cambridge University Press, Cambridge, UK, 2000.

[58] I. V. Markov. *Crystal Growth for Beginners: Fundamentals of Nucleation, Crystal Growth and Epitaxy*. World Scientific, Singapore, 1995.

[59] F. Schreiber. *Physica Status Solidi A*, 201:1037, 2004.

[60] J. Locklin and Z. Bao. *Analytical and Bioanalytical Chemistry*, 384:336, 2006.

[61] Z. Y. Zhang, X. Chen, and M. G. Lagally. *Physical Review Letters*, 73:1829, 1994.

[62] A. J. Salih, S. P. Lau, J. M. Marshall, J. M. Maud, W. R. Bowen, N. Hilal, R. W. Lovitt, and P. M. Williams. *Applied Physics Letters*, 69:2231, 1996.

[63] F. J. Meyer zu Heringdorf, M. C. Reuter, and R. M. Tromp. *Applied Physics A*, 78:787, 2004.

[64] M. Oehzelt, R. Resel, C. Suess, R. Friedlein, and W. R. Salaneck. *Journal of Chemical Physics*, 124:54711, 2006.

[65] J. B. Koo, S. H. Kim, J. H. Lee, C. H. Ku, S. C. Lim, and T. Zyung. *Synthetic Metals*, 156:2, 2006.

[66] R. Ruiz, B. Nickel, N. Koch, L. C. Feldman, R. F. Haglund, A. Kahn, F. Family, and G. Scoles. *Physical Review Letters B*, 67:125406, 2003.

[67] A. G. Richter, M. K. Durbin, C. J. Yu, and P. Dutta. *American Chemical Society*, 14:5980, 1998.

[68] M. Fanetti, L. Gavioli, M. Sancrotti, and M. G. Betti. *Applied Surface Science*, 252:5568, 2006.

[69] D. S. Park, S. J. Kang, H. J. Kim, M. J. Jang, M. Noh, K. H. Yoo, C. N. Whang, Y. S. Lee, and M. H. Lee. *Journal of Vacuum Science and Technology B*, 23:926, 2005.

[70] W. K. Burton, N. Cabrera, and F. C. Frank. *Philosophical Transactions of the Royal Society of London Series A*, 243:299, 1951.

[71] J. A. Venables, G. D. T. Spiller, and M. Hanbucken. *Reports on Progress in Physics*, 47:399, 1984.

[72] D. L. Smith. *Thin Film Deposition: Principles and Practice*. McGraw Hill Inc., New York, 1995.

[73] L. Zuppiroli, S. Pratontep, M. Brinkmann, and F. Nuesch. *Physical Review Letters B*, 69:165201, 2004.

[74] D. Sanvitto, M. De Seta, and F. Evangelisti. *Surface Science*, 452:191, 2000.

[75] M. Mobus and N. Karl. *Thin Solid Films*, 215:213, 1992.

[76] F. Biscarini, P. Samori, A. Lauria, P. Ostoja, R. Zamboni, C. Taliani, P. Viville, R. Lazzaroni, and J. L. Bredas. *Thin Solid Films*, 284:439, 1996.

[77] F. Biscarini, P. Samori, O. Greco, and R. Zamboni. *Physical Review Letters*, 78:2389, 1997.

[78] K. O. Lee and T. T. Gan. *Chemical Physics Letters*, 51:120, 1977.

[79] T. Minakata, H. Imai, and M. Ozaki. *Journal of Applied Physics*, 72:4178, 1992.

[80] J. Lee, J. H. Kim, and S. Im. *Journal of Applied Physics*, 95:7, 2004.

[81] C. K. Chiang, C. R. Fincher, Y. W. Park, and A. J. Heeger. *Physical Review Letters*, 39:1098, 1977.

[82] D. De Caro, M. Basso-Bert, J. Sakah, H. Casellas, J. P. Legros, L. Valade, and P. Cassoux. *Chemistry of Materials*, 12:587, 2000.

[83] D. Jerome, A. Mazaud, M. Ribault, and K. Bechgaard. *Journal of Physics Letters*, 41:L95, 1980.

[84] M. Shtein, P. Peumans, J. B. Benziger, and S. R. Forrest. *Advanced Materials*, 16:1615, 2004.

[85] H. Yang, T. J. Shin, M. M. Ling, K. Cho, C. Y. Ryu, and Z. Bao. *Journal of American Chemical Society*, 127:11542, 2005.

[86] A. C. Mayer, R. Ruiz, R. L. Headrick, A. Kazimirov, and G. G. Malliaras. *Organic Electronics*, 5:257, 2004.

[87] A. C. Durr, F. Schreiber, K. A. Ritley, V. Kruppa, J. Krug, H. Dosch, and B. Struth. *Physical Review Letters*, 90:016104, 2003.

[88] H. C. Kang and J. W. Evans. *Surface Science*, 271:1, 1992.

[89] J. W. Evans. *Physical Review B*, 43:5, 1991.

[90] I. Yamada, H. Takaoka, H. Usui, and T. Takagi. *Journal of Vacuum Science and Technology A*, 4:722, 1986.

[91] E. Hendell, U. Even, T. Raz, and R. D. Levine. *Physical Review Letters*, 74:2670, 1995.

[92] H. Usui, I. Yamada, and T. Takagi. *Journal of Vacuum Science and Technology A*, 4:52, 1998.

[93] D. Freedman and T. Arias. Cluster assimilation and collision filtering on metal oxide surfaces. http://www.arxiv.org/abs/comd-mater/0606014.

[94] A. Fleet, D. Dale, Y. Suzuki, and J. D. Brock. *Physical Review Letters*, 94:036102, 2005.

[95] J. Krug. *Journal of statistical physics*, 87:505, 1997.

[96] A. C. Mayer, A. Kazimirov, and G. G. Malliaras. *Physical Review Letters*, 97:105503, 2006.

[97] C. C. Mattheus, A. B. Dros, J. Bass, G. T. Oostergetel, A. Meetsma, J. L. de Boer, and T. T. M. Palstra. *Synthetic Metals*, 138:475, 2003.

[98] W. C. Marra, P. Eisenberger, and A. Y. Cho. *Journal of Applied Physics*, 50:6927, 1979.

[99] H. C. W. Beijerinck and N. F. Verster. *Physica 111C*, page 327, 1981.

[100] D. Choudhary, P. Clancy, R. Shetty, and F. Escobedo. *Advanced Functional Materials*, 16:1768, 2006.